

Fast coalescent-based computation of local branch support from quartet frequencies

Erfan Sayyari¹ and Siavash Mirarab^{*,1}

¹Department of Electrical and Computer Engineering, University of California at San Diego, 9500 Gilman Drive, La Jolla, CA 92093

***Corresponding author:** E-mail: smirarab@ucsd.edu.

Abstract

Species tree reconstruction is complicated by effects of Incomplete Lineage Sorting (ILS), commonly modeled by the multi-species coalescent model. While there has been substantial progress in developing methods that estimate a species tree given a collection of gene trees, less attention has been paid to fast and accurate methods of quantifying support. In this paper, we propose a fast algorithm to compute quartet-based support for each branch of a given species tree with regard to a given set of gene trees. We then show how the quartet support can be used in the context of the multi-species coalescent model to compute i) the local posterior probability that the branch is in the species tree and ii) the length of the branch in coalescent units. We evaluate the precision and recall of the local posterior probability on a wide set of simulated and biological data, and show that it has very high precision and improved recall compared to multi-locus bootstrapping. The estimated branch lengths are highly accurate when gene trees have little error, but are underestimated when gene tree estimation error increases. Computation of both branch length and local posterior probability is implemented as a new feature in ASTRAL.

Key words: Incomplete lineage sorting, multi-species coalescent, quartet-based methods, ASTRAL, posterior probability, local support

Introduction

The multi-species coalescent model (MSC) of Rannala and Yang (2003) has emerged as the standard method used for reconstructing species trees in presence of gene tree discordance due to Incomplete Lineage Sorting (ILS) (Degnan and Rosenberg, 2006; Maddison, 1997). Many methods have been developed to estimate species trees under the MSC (e.g., Bryant *et al.*, 2012; Chifman and Kubatko, 2014; Heled and Drummond, 2010; Mirarab *et al.*, 2014c), and the most scalable family of these methods are based on a two-step process where gene trees are first estimated independently for each gene, and are then combined to build the species tree using a *summary method*. Many of the summary methods are statistically consistent and thus converge in probability to the true species tree as the number of input error-free gene trees increases; examples of consistent methods include ASTRAL (Mirarab and Warnow,

2015; Mirarab *et al.*, 2014a), BUCKy-population (Larget *et al.*, 2010), GLASS (Mossel and Roch, 2010), MP-EST (Liu *et al.*, 2010), NJst and ASTRID (Liu and Yu, 2011; Vachaspati and Warnow, 2015), and STAR (Liu *et al.*, 2009). While some methods (e.g., MP-EST) can estimate branch lengths in coalescent units, others only infer the topology. The traditional concatenation approach (where all genes are put together in a supermatrix) can produce high support for incorrect branches (Kubatko and Degnan, 2007; Roch and Steel, 2014), and a main goal of statistically consistent summary methods is to address this shortcoming. However, despite the progress in developing methods for species tree reconstruction, little attention has been paid to methods of calculating support.

Bayesian methods (e.g., Heled and Drummond, 2010; Liu, 2008) readily provide support but remain computationally challenging. Calculating support through bootstrapping (Felsenstein, 1985), while still computationally expensive, is not prohibitively slow and is easily parallelizable. Seo *et al.* (2005) proposed a multi-locus bootstrapping (MLBS) procedure that produces bootstrap replicates by first resampling genes and then sites within those sampled genes. Seo (2008) later studied the accuracy of the MLBS approach in the context of distance-based tree reconstruction for 4-taxon trees, and explored other strategies where only genes or only sites were resampled, or where parameter distributions were centered and pivoted. These earlier works did not consider ILS as the cause of discordance; nor did they use summary methods. Nevertheless, the community has adopted MLBS as a standard way of estimating support using ILS-aware summary methods; most biological studies using summary methods rely on site-only or site+gene MLBS (e.g., Jarvis *et al.*, 2014; Prum *et al.*, 2015; Song *et al.*, 2012; Wickett *et al.*, 2014).

Recently, Mirarab *et al.* (2014b) studied the reliability of MLBS support values as a measure of accuracy in simulation studies, and documented both under-estimation and over-estimation of support (for low and high support branches, respectively) using MP-EST (Liu *et al.*, 2010) and supertree methods such as MRP (Ragan, 1992) and MRL (Nguyen *et al.*, 2012). Mirarab *et al.* (2014b) also observed better species tree accuracy when a summary method was run directly on ML gene trees, compared to running the summary method on bootstrapped gene trees first and then taking a consensus. This observation led to the conjecture that MLBS might give biased estimates of the support. Furthermore, Bayzid *et al.* (2015) found in simulation studies that false positive branches can sometimes have high MLBS support and that many true branches tend to have low support. Obtaining low support for true branches should not be a cause of concern if lack of support is caused by insufficient data; however, when low support is caused by underestimation, we need better methods of quantifying support.

In this paper, we show that using expectations of the MSC on four taxa (quartets), we can derive support values that are more precise and more powerful than MLBS, and are faster to compute. Under the MSC, quartet trees do not have anomaly zones (Allman *et al.*, 2011; Degnan, 2013), meaning that the most probable gene tree is identical to the species tree for any quartet. Exploiting this property, some summary methods break up gene trees into quartet trees. For example, ASTRAL (Mirarab and Warnow, 2015), a new summary method used in many recent studies (e.g., Andrade *et al.*, 2015; Giarla and Esselstyn, 2015; Grover *et al.*, 2015; Hosner *et al.*, 2011; Laumer *et al.*, 2015; Prum *et al.*, 2015; Streicher *et al.*, 2015; Wickett *et al.*, 2014), finds the species tree that shares the maximum number of induced quartet trees with gene trees.

We introduce a new method for computing support for species tree branches with regard to a set of unrooted gene trees by calculating Bayesian posterior probabilities. Our support values, which we call *local posterior probabilities*, are computed based on gene tree quartet frequencies. For each internal branch of the given species tree, we *assume* that the four *sides* of the branch (Fig. 1) are correct, and therefore three topologies are possible around that branch. We introduce a fast algorithm to compute a *quartet support* for each of those three alternatives in $\Theta(kn)$ time (where n is the number of species and k is the number of genes). We then use the quartet support for each alternative topology to derive the posterior probability that it is the correct species topology. Besides producing measures of support, quartet frequencies can be used to derive estimates of internal branch lengths in coalescent units.

Our calculation of posterior probabilities is analogous to characterizing a biased die. If we toss a three-faceted biased die k times, our belief in whether the die is biased towards a certain side should depends on the number of tosses and also on the bias of the die (less bias requires more tosses). Similarly, a short branch in the species tree will results in lots of discordance, and will need many genes to resolve it with high confidence. On the other hand, considering only the MSC and ignoring issues such as long branch attraction, long branches can be easily reconstructed confidently even with few genes.

We show using simulated and empirical datasets that local posterior probabilities estimated by our approach are reliable measures of accuracy. We show that very few highly supported branches are incorrect. Moreover, with a sufficient number of genes, most correct branches have high support. Importantly, we test our posterior probabilities under conditions where assumptions of our model are violated, and show that they remain reliable. Our method is available as part of ASTRAL¹ (which now estimates species tree topologies, branch lengths, and local posterior probabilities).

¹Publicly available on the development branch at <https://github.com/smirarab/ASTRAL/tree/blen>; will be merged with the main branch upon acceptance.

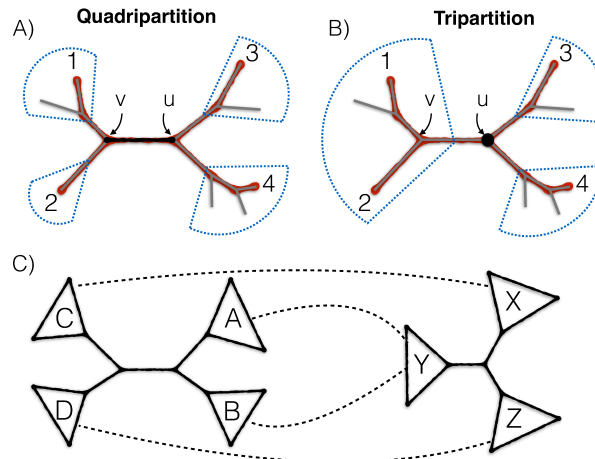


FIG. 1. Quadripartition and tripartitions. A) An internal branch (black, in the middle) divides the set of leaves into a quadripartition. A quartet of leaves $\{1, 2, 3, 4\}$ induces a quartet tree (in red) with two internal nodes that map to two nodes in the larger tree (here, u and v). B) An internal node, here u , divides leaves into a tripartition; a selection of two leaves from one side and one from each remaining side gives a quartet mapped to that tripartition. Each quartet tree also maps to a second tripartition (v). C) An example mapping between a quadripartition and a tripartition; 12 such mappings exist. Note that by finding all quartets of the form $(a, b, c, d); a \in A \cap Y, b \in B \cap Y, c \in C \cap X, d \in D \cap Z$, we can find all quartets around the quadripartition that are mapped to the tripartition with this mapping.

New Approaches

Definitions: Throughout this paper, we only consider unrooted trees. Let \mathcal{L} be the set of n leaves (i.e., taxa). Each branch of a tree T creates a bipartition on \mathcal{L} , and we say that each of the two partitions is a *cluster* in T . Each *internal* branch divides \mathcal{L} into four clusters, creating a quadripartition (Fig. 1). Similarly, an internal node divides \mathcal{L} into three clusters, creating a tripartition (Fig. 1). Any quartet q of taxa induces a quartet tree t on T . The two internal nodes of t correspond to two internal nodes in T . When those two internal nodes are the two sides of a single branch in T , we say that the quartet q is *around* that branch. The set of quartets around a given quadripartition can be built by enumerating all selections of one leaf from each of its four clusters.

Problem statement: We are given a set of k gene trees evolved on an unknown true binary species tree according to the MSC model. Our aim is to *score* a given internal branch represented as a quadripartition Q to estimate:

- 1) the probability that Q is in the true species tree, assuming clusters of Q are each correct,
- 2) the length of Q in coalescent units, assuming Q is a correct branch in the species tree.

Assumptions: We assume evolution is tree-like and true gene trees differ from the species tree only due to ILS, as modeled by the MSC. We also assume we are given an unbiased sample of true gene trees. On real data, we need to instead estimate gene trees from sequence data, and further, it is not always clear that our sample is unbiased, nor that gene trees are generated by the MSC.

Importantly, we further assume that all four clusters around the branch we are scoring are correct. This assumption, which we refer to as the *locality assumption*, makes our computations tractable for large datasets. Similar assumptions have been made in past for fast calculation of local support in the context of maximum likelihood (ML) tree reconstruction from sequence data; e.g., aLRT in PhyML (Guindon *et al.*, 2009) and SH-like support in FastTree-II (Price *et al.*, 2010). Note that to test our method, we use data that violate the locality assumption and we also use estimated gene trees in addition to true gene trees generated by the MSC.

Calculation of local posterior probability

Quartet trees: Our approach is based on analyzing quartets defined around the branch Q . For any quartet of leaves around Q , we have three possible topologies, which we will call t_1 , t_2 , and t_3 . In the MSC model, the quartet topology found in the true species tree has the highest probability of appearing in gene trees (Allman *et al.*, 2011), and the two alternative topologies have identical probabilities. Furthermore, if the total branch length (in coalescent units) between the two internal nodes of the quartet is d , the probability of the dominant quartet topology in gene trees is $\theta = 1 - \frac{2}{3}e^{-d}$, and the probabilities of both alternative topologies are $\frac{1-\theta}{2} = \frac{1}{3}e^{-d}$.

We refer to the number of times t_1 , t_2 , and t_3 are induced in gene trees as *quartet frequencies*, shown as $F = (f_1, f_2, f_3)$; note $\sum_1^3 f_j = k$. In the MSC model, conditioned on the species tree, gene trees are independent; Thus, F follows the multinomial distribution with parameters θ , $\frac{1-\theta}{2}$, $\frac{1-\theta}{2}$, where θ is for the species tree topology, and $\frac{1-\theta}{2}$ for the alternative topologies. A similar multinomial model is used in the maximum pseudo-likelihood approach of Liu *et al.* (2010) for triplets.

Multiple quartets: There are $m = \prod_1^4 m_i$ quartets around branch Q , where m_i is the size of a cluster of the quadripartition of Q . Note that we can rearrange clusters of Q to obtain two alternative quadripartition, which we call Q_2 and Q_3 . Let $F_i = (f_{1i}, f_{2i}, f_{3i})$, $1 \leq i \leq m$ be quartet frequencies for all m quartets around branch Q such that f_{1i} values correspond to the topology of Q (i.e., the topology we are scoring), and f_{2i} and f_{3i} correspond to Q_2 and Q_3 . We need to decide how to use all F_i values.

F_i variables are identically distributed. One approach is to assume they are also all independent, and model $(\sum f_{1i}, \sum f_{2i}, \sum f_{3i})$ as $m \times k$ observations from a single multinomial distribution. The independence assumption would clearly be incorrect; topologies of different quartets around a branch heavily depend on each other (see Fig. S14 for an example). A big problem with the independence assumption is that it inflates confidence because the number of observations (i.e., die tosses) becomes $m \times k$ instead of k ,

thereby greatly increasing posterior probabilities (note $m \geq n-3$). Moreover, the dependence of various quartets on each other is intricate and hard to model.

To avoid inflating our posterior values through an independence assumption, we take the opposite conservative approach. We assume that there is a hidden random variable $F^* = (f_1^*, f_2^*, f_3^*)$ giving a single set of quartet frequencies around Q and treat each F_i as a noisy estimates of F^* . In the die analogy, we toss k times, and for each toss, we read the outcome m times, each time with some noise. Thus, F^* follows a multinomial distribution, with k tries (irrespective of m) and can be empirically estimated by averaging:

$$f_j^* = \frac{\sum_1^m f_{ji}}{m} \quad \text{for } j \in \{1, 2, 3\} \quad (1)$$

At the end of this section, we will introduce an efficient $\Theta(nk)$ algorithm to compute F^* , but for now we assume F^* is computed.

Lemma 1. *Let $(\theta_1, \theta_2, \theta_3)$ denote parameters of the true multinomial distribution generating F^* . Note $\sum_1^3 \theta_i = 1$ and the two lower θ_i s are identical, and recall f_1^* corresponds to the topology of Q .*

$$Pr(\theta_1 > \frac{1}{3} | F^*) = \frac{\int_{\frac{1}{3}}^1 Pr(F^* | \theta_1 = t) Pr(\theta_1 = t) dt}{Pr(F^*)} \quad (2)$$

with likelihood term:

$$Pr(F^* | \theta_1 = t) = \Gamma t^{f_1^*} \left(\frac{1-t}{2}\right)^{k-f_1^*} \quad (3)$$

where $\Gamma = \frac{\Gamma(k+1)}{\prod_1^3 \Gamma(f_j^* + 1)}$, and marginal probability:

$$\begin{aligned} Pr(F^*) &= \sum_{j=1}^3 \int_{\frac{1}{3}}^1 Pr(F^* | \theta_j = t) Pr(\theta_j = t) dt \\ &= \Gamma \sum_{j=1}^3 \int_{\frac{1}{3}}^1 t^{f_j^*} \left(\frac{1-t}{2}\right)^{k-f_j^*} Pr(\theta_j = t) dt. \end{aligned} \quad (4)$$

Proof is given in supplementary material. Q is in the species tree iff $\theta_1 > \frac{1}{3}$; thus, with Lemma 1 and a prior we can compute the posterior probability.

Prior: In absence of extra reliable information about the species tree topology, which is the most common scenario, the use of an uninformative prior is justified. An uninformative prior would require that the three topologies are equally likely (i.e., $Pr(\theta_1 > \frac{1}{3}) = Pr(\theta_2 > \frac{1}{3}) = Pr(\theta_3 > \frac{1}{3}) = \frac{1}{3}$). Based on Theorem 3.3 from Stadler and Steel (2012), we can prove (Supplementary material):

Lemma 2. *If the species tree is generated using the Yule process with rate λ , branch lengths are exponentially distributed, and for $t \geq \frac{1}{3}$:*

$$Pr(\theta_j = t) = \lambda \left(3 \frac{1-t}{2}\right)^{2\lambda-1} \quad (5)$$

In the rest of this manuscript, we use (2) as prior for all θ_j parameters. Note that setting $\lambda = \frac{1}{2}$ gives a flat prior. Furthermore, note that our assumption is that branch lengths in coalescent units are generated by the Yule process; this can be achieved if population sizes remain constant throughout the tree.

Local posterior probability: We now conclude:

Theorem 1 *Given 1) a set of k gene trees generated by the MSC on a model species tree generated by the Yule process with rate λ and 2) an internal branch represented by a quadripartition Q where the four clusters around Q are each present in the species tree, let $F^* = (f_1^*, f_2^*, f_3^*)$ be the average quartet frequencies around Q (where f_1^* corresponds to the topology of Q); the local posterior probability that the species tree has the topology given by Q is:*

$$Pr(Q|F^*) = \frac{h(f_1^*)}{h(f_1^*) + 2f_2^* - f_1^* h(f_2^*) + 2f_3^* - f_1^* h(f_3^*)} \quad (6)$$

where

$$h(x) = \mathbf{B}(x+1, k-x+2\lambda)(1 - I_{\frac{1}{3}}(x+1, k-x+2\lambda)).$$

Here, $\mathbf{B}(\alpha, \beta)$ is the beta function, and I_x is the regularized incomplete beta function.

Proof (sketch). F^* follows a multinomial distribution with parameters $(\theta_1, \theta_2, \theta_3)$. Lack of anomaly zones for unrooted quartets, shown by (Allman *et al.*, 2011) means that Q is in the species tree iff $\theta_1 > \frac{1}{3}$. Thus, by Lemma 1 we can use (2), (3), and (4) to compute the local posterior probability of Q . By the assumption that (coalescent unit) branch lengths in the species tree are generated by the Yule process, and by Lemma 2, our prior becomes the euqation shown in (5). Calculation of (6) follows from manipulating (2), (3), and (4), as detailed in the Supplementary material. \square

Examples: The local posterior probability (pp) is a function of the number of genes and the quartet frequency of a branch. As Figure 2 shows, a branch that appears in 40% of gene trees has a low 66.1% pp if 50 gene trees given (and alternative topologies are equally frequent); however, with 200 or 500 genes, the same branch will have 93.0% or 99.7% pp, respectively. Thus, a high discordance branch where 60% of genes do not agree with the species tree can still be resolved with high confidence given enough genes. Moreover, the posterior probability is affected not just by the frequency of the topology being scored, but also by the frequency of the two alternatives. For example, if our branch of interest appears in 40% of

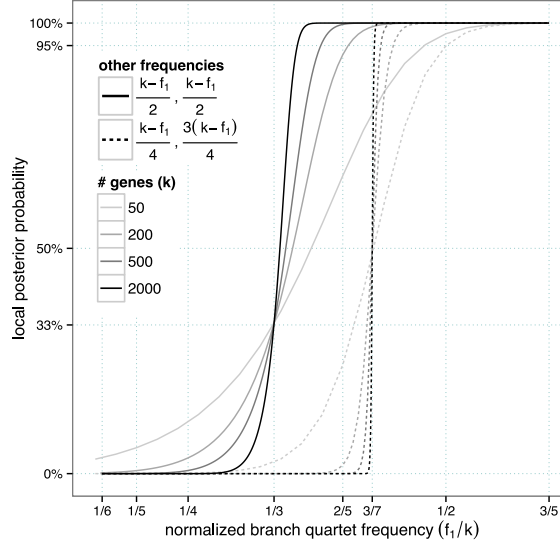


FIG. 2. Local posterior probability of a branch as a function of its normalized quartet support for varying numbers of genes. Solid lines: alternative topologies have equal frequency (thus, conform to expectations of the MSC for x greater than $1/3$); dotted lines: alternative topologies don't have equal frequency (contrary to the MSC).

gene trees, but a second alternative appears in three-quarters of the remaining genes (i.e., 45% of genes), the branch with 40% frequency has only a 1.90% pp (Fig. 2).

Calculation of branch length

Given the true parameter θ for a correct branch, its length in coalescent units (Degnan and Rosenberg, 2006) is simply $-\ln \frac{3}{2}(1-\theta)$. Thus, we can prove (see Supplementary material):

Theorem 2 *Under conditions of Theorem 1, and assuming the branch represented by Q is in the species tree, the ML estimate for its length is $-\ln \frac{3}{2}(1-\frac{f_1^*}{k})$ and the MAP estimate is $-\ln \frac{3}{2}(1-\frac{f_1^*}{k+2\lambda})$ when $3f_1^* \geq k$ and $3f_1^* \geq k+2\lambda$, respectively; otherwise, both ML and MAP are zero.*

Calculation of quartet support

We now discuss how F^* defined in (1) can be efficiently computed. Note that in the worst case, there can be $\Theta(n^4)$ quartets around a single branch. Thus, simply enumerating all f_{ij} values and then getting the average can be very slow.

As noted before, each quartet around Q has each of its four leaves drawn from a different cluster of Q . Recall also that internal nodes of a tree produce a tripartition, and as Mirarab *et al.* (2014a) pointed out, any selection of two leaves from one side of the tripartition and one leaf from each remaining side gives a quartet tree mapped to that tripartition (Fig. 1). Let $\psi(Q)$ and $\psi(R)$ give the set of quartet trees around a quadripartition and mapped to a tripartition, respectively. Any quartet tree around Q that is induced by a gene tree will be mapped to two internal nodes in that gene tree (Fig. 1). Thus,

$$f_1^* = \frac{1}{2m} \sum_{g=1}^k \sum_{u=1}^{n-2} |\psi(R_u^g) \cap \psi(Q)| \quad (7)$$

where R_u^g is a tripartition for node u in gene tree g and m is the number of quartets around Q .

We can efficiently compute the number of quartet topologies around Q that appear also in a tripartition R (i.e., $|\psi(R_u^g) \cap \psi(Q)|$) without computing $\psi(\cdot)$ sets. We define a mapping between clusters around Q to clusters in R : map two sister clusters in Q to a cluster in R , and map the remaining two clusters in Q to the remaining two clusters in R (Fig. 1). For example, let $Q = A, B | C, D$ and $R = X | Y | Z$; a possible matching is to map A and B to Y , C to X , and D to Z . There are 12 possible matchings between Q and R . For each matching, we can compute the number of quartet trees around Q that appear in R by multiplying the sizes of the intersection of pairs of clusters in Q and R that are mapped to each other. By enumerating all 12 matching and summing the resulting numbers, we get $|\psi(R_u^g) \cap \psi(Q)|$. Since finding the intersection of two clusters requires $\Theta(n)$, computing (7) would require $O(n^2k)$ running time. However, we can do better. Mirarab and Warnow (2015) have introduced a $\Theta(nk)$ algorithm to compute a sum similar to (7) for scoring a tripartition, based on a postorder traversal of gene trees (instead of analyzing each R_u separately). This algorithm can be adopted here to compute (7) in $\Theta(nk)$ (see Fig. S13 for the algorithm). Since scoring a tree requires scoring $n-3$ branches,

Theorem 3 *Computing branch lengths and local posterior probabilities of a tree requires $\Theta(n^2k)$ time.*

Other considerations

Handling missing data and unresolved gene trees requires extra care. When gene trees have missing data, to compute (7), instead of setting m to the number of quartets around Q , we need to set it to the average number of quartets present in gene trees (i.e., $\frac{1}{k} \sum_1^3 f_j^*$). Moreover, missing data can cause some genes to miss *all* quartets around Q ; to account for this, we allow a different k for each branch, and set it to the number of genes that include at least one of the quartets around Q . To handle unresolved gene trees, similar to ASTRAL-II, we need to score the quadripartition against all $\binom{d}{3}$ tripartitions around a polytomy with degree d .

Our methods are implemented in ASTRAL, using the Colt package for mathematical computations (Hoschek, 2002).

Materials and Methods

Datasets

We use both simulated and biological datasets.

Simulated data

We use two sets of simulated datasets from previous publications: the 200-taxon dataset (called A-200 here) from Mirarab and Warnow (2015) and an avian dataset with 48 taxa from Mirarab *et al.* (2014c). A-200 enables us to test accuracy under heterogeneous conditions with many species, and the avian dataset is used to compare local posterior against MLBS. For both datasets, gene trees are simulated

Table 1. Properties of simulated datasets.

	Cond.	n	k	R	ILS	GE	SE
A-200	Low-ILS	201	1000	100	15%	25%	6%, 4%, 3%
A-200	Med-ILS	201	1000	100	34%	31%	9%, 6%, 4%
A-200	High-ILS	201	1000	100	69%	47%	19%, 10%, 6%
Avian	1500bp	48	1000	20	47%	31%	5%
Avian	1000bp	48	1000	20	47%	39%	6%
Avian	500bp	48	1000	20	47%	54%	8%
Avian	250bp	48	1000	20	47%	67%	15%

n: number of species; *k*: maximum number of genes (A-200 also has 50 and 200); *R*: number of replicates; *ILS*: average normalized RF (Robinson and Foulds, 1981) distance (AD) between the true species tree and true gene trees; *GE*: AD between true and estimated gene trees; *SE*: AD between true and ASTRAL species trees (for A-200, with 50, 200, and 1000 genes, respectively).

using the MSC, and their branch lengths are then adjusted to be in substitution units and to deviate from strict molecular clock. Sequence data are next simulated on the modified gene trees using GTR+ Γ , and ML gene trees are estimated from the data. On the avian dataset, bootstrapped gene trees are also available. For both datasets, in addition to the true species tree, we have species trees estimated using ASTRAL and NJst given estimated gene trees, and concatenation using ML. We show results for ASTRAL and true species tree here, and refer the reader to supplementary material for NJst and concatenation.

A-200 : This 201-taxon datasets (200 ingroups plus an outgroup, treated like other taxa here) are simulated using SimPhy (Mallo *et al.*, 2015), and has three levels of ILS (Table 1), with true discordance that ranges from very low to very high (Fig. S1). Each replicate of the simulation has its own species tree, and the ILS level is controlled by changing the tree length (500k, 2M, and 10M generations). Mirarab and Warnow (2015) generated species trees using the Yule process with two speciation rates (10^{-6} and 10^{-7} per generation) for each tree length, but here we combine the two rates into one dataset to get twice the number of replicates. SimPhy automatically introduces deviation from the strict clock by drawing species, gene, and gene/species specific rate multipliers from predefined distributions. Similarly, the number of sites for each gene is randomly chosen. See Mirarab and Warnow (2015) for details. ML Gene trees are estimated using FastTree-II (Price *et al.*, 2010), with a wide range of estimation error (Table 1 and Fig. S1). Species trees are estimated based on all 1000 genes per replicate, or on subsets of 200 or 50 genes. The ASTRAL species trees error for various datasets ranges between average 3% and 19% (Table 1).

Avian: The avian dataset has 48 taxa, and is simulated to emulate the whole-genome dataset of Jarvis *et al.* (2014), possibly overestimating the true amount of ILS (Gatesy and Springer, 2014; Mirarab *et al.*, 2014c). Here, we use four conditions, with 20 replicates that each includes 1000 genes, all simulated based on the same avian-like species tree. Our four conditions differ in terms of the number

of sites per gene (250bp, 500bp, 1000bp, or 1500bp), creating varying levels of gene tree estimation error (Table 1). ML Gene trees are estimated using RAxML (Stamatakis, 2014), and 200 replicates of bootstrapping are performed. Average ASTRAL species tree error ranges from 5% to 15%, depending on the gene tree error (Table 1). We used site-only MLBS to get BS support values. A single branch in our true tree was extremely short (almost a polytomy, with a length of 10^{-6}). When discussing branch length accuracy, we ignore that branch; results including that branch are also shown for completeness.

Biological dataset:

We re-analyze four published biological datasets: the 103-taxon 424 gene plant dataset of Wickett *et al.* (2014), the 46-taxon 310 gene angiosperm dataset of Xi *et al.* (2014), the 48-taxon 2022 supergene tree (i.e., binned) dataset of Jarvis *et al.* (2014), and finally the 201-taxon 256 gene avian dataset of Prum *et al.* (2015).

Evaluation procedure

We study three questions in our evaluation:

- How accurate are branch lengths and support values when assumptions of our model are met?
- How do violations of the model assumptions impact the result?
- How do local posterior probabilities compare to site-only MLBS?

To answer these questions, we use both true gene trees and estimated gene trees to score both true and estimated species trees. For every internal branch in the species tree being scored, we also score its two alternative topologies. For example, if branch $AB|CD$ (Fig. 1) appears in the species tree, we also score $AD|BC$ and $AC|BD$. In all analyses, we use the Yule prior with $\lambda = \frac{1}{2}$. Thus, our prior is uninformative and results in flat distributions for θ_j parameters.

With true species trees and true gene trees, all model assumptions are met. When estimated gene trees are used instead of true gene trees, we violate the assumption that input gene trees follow expectations of the MSC. When estimated species tree are scored, the locality assumption is potentially violated (i.e., each of the four clusters around a branch may be incorrect).

Measurement

Posterior: Despite the long-standing debate about correct interpretations of various measures of support (e.g., Felsenstein and Kishino, 1993; Hillis and Bull, 1993; Salichos and Rokas, 2013; Susko, 2009), biologists typically use support to judge branch reliability. A common practice is to ignore branches below a certain threshold of support and only interpret the remaining branches as biologically meaningful (0.95 for posterior and 70% for bootstrap are often used). Our evaluation procedure takes a

Table 2. Precision (and recall) of local posterior probabilities on A-200 dataset

	k	True species tree				ASTRAL species tree			
		True gene tree		Estimated gene tree		True gene tree		Estimated gene tree	
		.99	.95	.99	.95	.99	.95	.99	.95
Low ILS	1000	100.0(98.3)	100.0(98.7)	98.6(94.6)	98.4(95.4)	98.8(98.4)	98.8(98.8)	98.0(95.1)	97.8(95.9)
Low ILS	200	100.0(95.9)	100.0(96.8)	99.1(90.2)	98.9(91.9)	98.9(96.2)	98.8(97.1)	98.7(90.6)	98.5(92.4)
Low ILS	50	100.0(91.1)	100.0(93.2)	99.6(81.0)	99.3(85.0)	98.7(91.6)	98.6(93.6)	99.4(81.6)	99.0(85.6)
Med ILS	1000	100.0(95.1)	100.0(96.2)	98.9(90.8)	98.7(92.4)	99.3(95.4)	99.2(96.6)	98.6(91.2)	98.4(92.8)
Med ILS	200	100.0(89.2)	100.0(91.3)	99.4(82.6)	99.2(85.7)	99.4(90.0)	99.4(92.1)	99.3(83.3)	99.0(86.5)
Med ILS	50	100.0(79.0)	99.9(83.2)	99.7(70.0)	99.5(75.2)	99.4(81.0)	99.2(85.2)	99.7(71.3)	99.5(76.6)
High ILS	1000	100.0(83.0)	100.0(86.0)	99.4(77.5)	99.2(81.3)	99.7(84.2)	99.6(87.1)	99.4(78.3)	99.2(82.1)
High ILS	200	100.0(67.3)	100.0(72.8)	99.8(60.3)	99.6(66.6)	99.8(69.6)	99.7(75.1)	99.8(61.9)	99.6(68.3)
High ILS	50	100.0(46.0)	99.8(55.0)	99.8(38.6)	99.6(47.7)	99.8(50.0)	99.4(59.7)	99.8(41.1)	99.6(50.6)

NOTE.—For local posterior probability thresholds 0.95 and 0.99, we show the precision and recall (shown parenthetically) when true or ASTRAL species trees are scored with true or estimated gene trees.

similar approach; we use varying thresholds of support and count the number of true and false branches with support at least equal to the threshold. For a threshold s , the measures we use are precision (the percentage of branches with support $\geq s$ that are correct), recall (the percentage of all true branches that have support $\geq s$), and false positive rate (FPR) (the percentage of all false branches that have support $\geq s$). We also draw the ROC curve (i.e., recall versus FPR).

MLBS and posteriors values are not directly comparable. Therefore, it is pointless to compare the precision or recall of MLBS and posterior for a given threshold. Instead, we use the ROC curve, which is agnostic to the exact interpretation of the threshold; it simply shows which method results in a better trade-off between false negative and false positive branches. Moreover, comparing to MLBS was only feasible on the avian dataset, where gene bootstrapping was doable. On the A-200 dataset (300 replicates each with 1000 genes of 201 taxa) bootstrapping was not computationally feasible.

Branch length: To compute branch length accuracy, we compare the true and the estimated length for the same branch. This can be done only for correct branches; thus, we measure the accuracy of estimated branch lengths only for the true species tree topology. We use the logarithmic (log) error defined as $\frac{1}{b} \sum_1^b |\log_{10}(w_i) - \log_{10}(\hat{w}_i)|$ (where b is the number of branches, and w_i and \hat{w}_i are the true and estimated branch lengths, respectively). We also plot log of estimated versus true values. In addition, we show the root mean squared error, defined as $\sqrt{\frac{1}{b} \sum_1^b (w_i - \hat{w}_i)^2}$.

Results

A-200 dataset

Posterior

True trees: When true species trees are scored with true gene trees, the precision of branches with 0.99 pp or higher is 100% for all model conditions, and is at least 99.8% for the 0.95 threshold (Table 2). Thus, there are very few false positive branches that have high local pp, a trend that continues if we

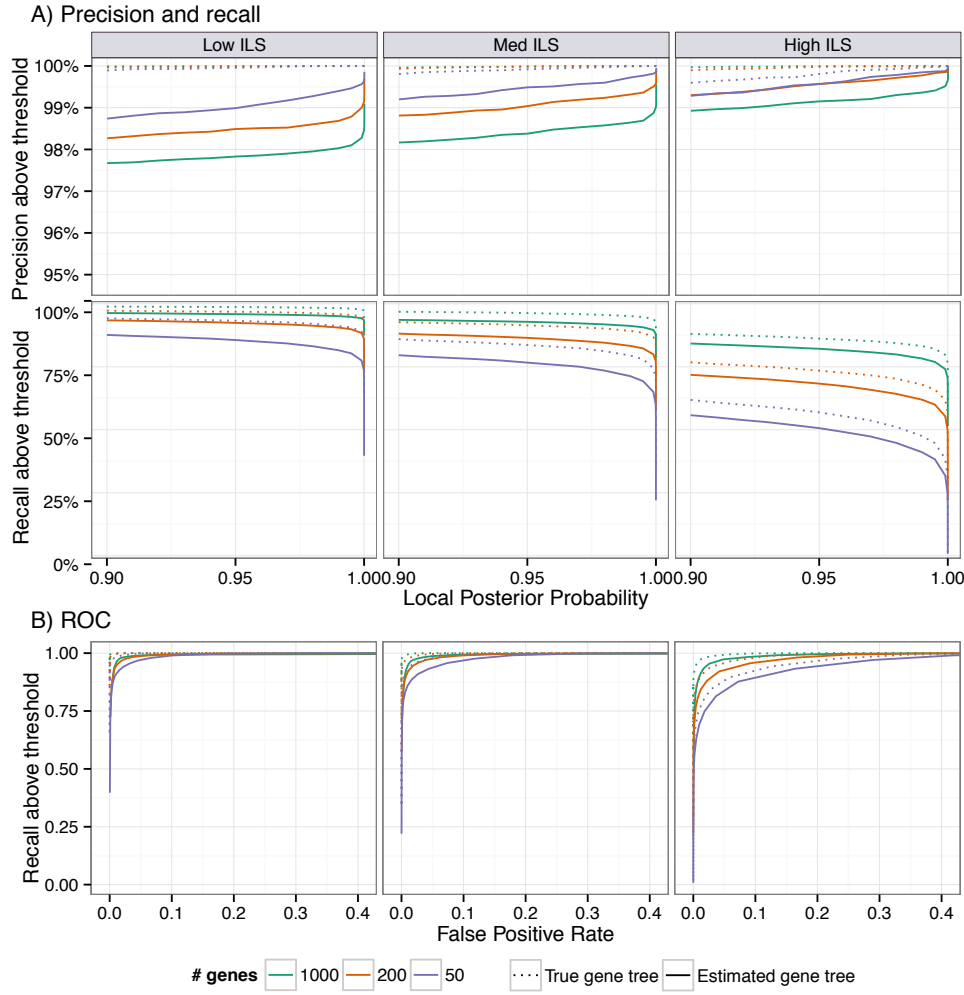


FIG. 3. Evaluation of local posterior probability on the A-200 dataset with ASTRAL species trees. See Figures S2-S4 for other species trees. A) Precision and recall of branches with local posterior probability above a threshold ranging from 0.9 to 1.0 using estimated gene trees (solid) or true gene trees (dotted). B) ROC curve (recall versus false positive rate) for varying thresholds (figure trimmed at 0.4 FPR). Columns show different levels of ILS.

further lower the threshold to 0.9 (Fig. S2). With the 0.99 threshold, the percentage of true branches that are recovered (recall) ranges from very high (98%) for the model condition with low ILS and 1000 gene trees to moderately low (46%) for the most challenging dataset with high ILS and only 50 genes (Table 2). As desired, increasing ILS and reducing the number of genes both reduce the recall while maintaining high precision (Fig. S2).

Estimated gene trees: When true species trees are scored on estimated gene trees instead of true gene trees, precision slightly drops from 100% to between 98.4% and 99.8%. The recall, however, is impacted more and is reduced by as much as 10% (Table 2 and Fig. S2). Thus, gene tree estimation error has a small impact on the precision but a substantial impact on the recall.

The impact of the threshold is also interesting. Going from the 0.99 to 0.95 threshold, as expected, recall improves (e.g., from 39% to 48% for high ILS, 50 genes) but reductions in the precision are very small (at most 0.3%). Thus, a 95% threshold results in meaningful improvements in the recall without

Table 3. Branch length accuracy on the A-200 dataset.

Dataset	k	True gt	Log Err	Est. gt	True gt	RMSE	Est. gt
Low ILS	1000	0.07	0.40	0.40	3.93	6.28	
Low ILS	200	0.11	0.40	0.40	4.51	6.22	
Low ILS	50	0.17	0.41	0.41	5.10	6.13	
Med ILS	1000	0.04	0.20	0.20	0.71	0.86	
Med ILS	200	0.08	0.21	0.21	1.25	0.99	
Med ILS	50	0.15	0.24	0.24	1.85	1.32	
High ILS	1000	0.06	0.15	0.15	0.03	0.13	
High ILS	200	0.11	0.18	0.18	0.07	0.15	
High ILS	50	0.18	0.23	0.23	0.15	0.18	

Logarithmic error (Log Err) and root mean squared error (RMSE) are shown for true species trees scored with true gene trees or estimated gene trees (Est. gt).

substantially sacrificing the precision. The ROC curves (Figs. 3B and S2) further explore the tradeoff between increasing recall and allowing false positive branches.

Estimated species trees: By scoring estimated species trees we study the impact of violating the locality assumption. We show results for ASTRAL here, but similar results are obtained with NJst and concatenation (Figs. S2 and S4).

Precision and recall values are remarkably similar between ASTRAL and true species trees when estimated gene trees are used (Table 2), indicating that moderate violations of the locality assumption have minimal impact. Comparing true and ASTRAL species trees, the precision is reduced at most by 0.6% while the recall is surprisingly increased, by up to 2.9%. The impact of violating locality assumptions is more pronounced when true gene trees are used. Once again, precision is reduced (by as much as 1.2%) and the recall is increased (up to 4.7%).

We note that in our analyses, deviations from the locality assumption are moderate but realistic, as most ASTRAL trees have relatively high accuracy (Table 1). The least accurate ASTRAL trees have 19% RF distance to the true species tree (50 genes and high ILS), which means 81% of the clusters in the estimated tree remain correct. Nevertheless, it is interesting that violating the locality assumption for up to 19% of clusters has minimal impact on the precision and positive impact on the recall.

Branch Length

The accuracy of branch lengths are dramatically impacted by gene tree estimation error, number of genes, and the amount of ILS (Table 3). With 1000 true gene trees, the logarithmic error is very low, ranging from 0.04 to 0.07 (which correspond to branches that on average are respectively 9% or 17% shorter or longer than true branches). As the number of genes is reduced, the logarithmic error predictably goes up, but with true gene trees, it never exceeds 0.18 (roughly corresponding to branches that are on average 50% too short/long). Moreover, with true gene trees, the error is largely unbiased, except perhaps for

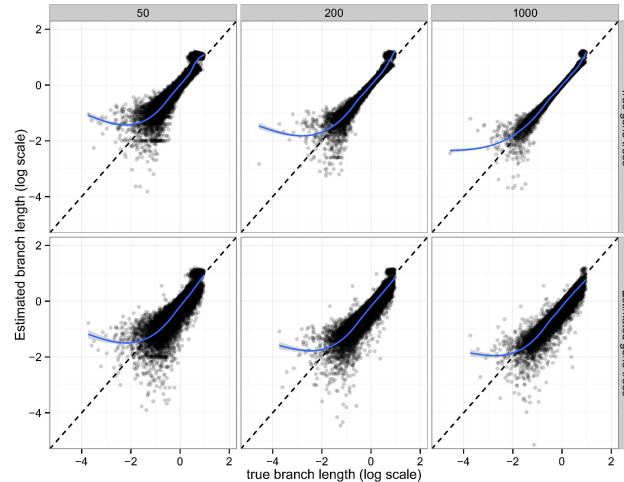


FIG. 4. Branch length accuracy on the A-200 dataset with Medium ILS. See Figs S7 and S8 for low and high ILS. The estimated branch length is plotted against the true branch length in log scale (base 10). Blue line: a fitted generalized additive model with smoothing (Wood, 2011).

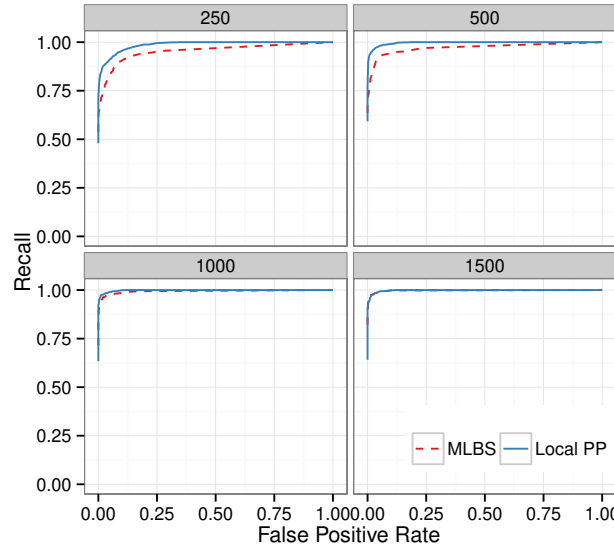


FIG. 5. ROC curve for the avian dataset based on MLBS and local posterior probability (PP) support values. Boxes show different numbers of sites per gene (controlling gene tree estimation error).

very short or long branches that are hard to estimate correctly with limited number of genes (Figs. 4 and S7-S8).

Branch length error dramatically increases when estimated gene trees are used. Low ILS conditions are impacted the most by gene tree error (Table 3 and Fig. S7). For example, with 1000 estimated gene trees and low ILS, log error is 0.4, corresponding to estimated branches that are on average 2.5 times too short or long. Moreover, the error is biased towards underestimation, especially for low ILS (Figs. 4, S7, and S8). These patterns are not surprising. As we will show, gene tree error tends to increase observed gene tree discordance; since branch lengths are impacted by observed discordance, this can result in underestimated branch lengths.

Table 4. Branch length accuracy for the avian dataset.

	True gt.	1500bp	1000bp	500bp	250bp
L	0.07(0.12)	0.16(0.21)	0.22(0.26)	0.37(0.42)	0.58(0.62)
R	1.35(1.33)	1.00(0.99)	1.14(1.13)	1.66(1.64)	2.19(2.16)

Logarithmic error (L) and root mean squared error (R) are shown for true species trees scored with true gene trees or estimated gene trees with various numbers of sites. A single extremely short branch (10^{-6}) was removed from the calculations, but error including that branch is shown parenthetically.

Avian

On the avian dataset, we compare local posterior probabilities against branch support generated using site-only MLBS with estimated gene trees and ASTRAL species trees. Here, we also study the impact of increasing levels of gene tree estimation error by decreasing the number of sites per gene from 1500bp to 250bp.

Posterior and MLBS

The precision of local posterior probability is 100% for the 0.99 threshold, regardless of the numbers of sites, but the recall ranges from 81% for the 1500bp model condition to 69% for 250bp (Table S1 and Figs. S5 and S6). Precision is at least 99.8% for the 0.95 threshold, and the recall is between 71.5% and 84.7%, depending on the model condition (an improvement of 2% to 5% compared to the 0.99 threshold). Lowering the support threshold all the way to 0.7 still retains at least 99.1% accuracy and increases the recall to between 78.3% and 91.4%. Therefore, the local posterior probabilities allow very few false positives with high support but also miss some true positives (and thus may be conservative).

Nevertheless, local posterior probabilities are less conservative than MLBS support values (i.e., have better recall). As the ROC curves (Fig. 5) show, for the same number of false positives branches, local posterior probabilities result in better recall than MLBS. This pattern is more pronounced for shorter alignments (which have increased gene tree error). For example, for the 250bp model condition, if we choose a support threshold that results in 0.01 false positive rate, with local posterior values, we still recover 84% of correct branches, whereas with MLBS, the same false positive rate results in retaining 70% of correct branches. Thus, for a desired level of precision, better recall can be obtained using local posterior probabilities.

Branch Length

Branch length accuracy on the avian dataset was a function of gene tree estimation error (Table 4). With true gene trees, branch length log error was only 0.07, corresponding to branches that are about 17% shorter or longer than the true branch. As gene tree estimation error increases with reduced number of sites (see Table 1 for gene tree error statistics), the branch length error also increases. Thus, while 1500bp genes give 0.16 log error, 250bp genes result in 0.58 error, which corresponds to branches that are on

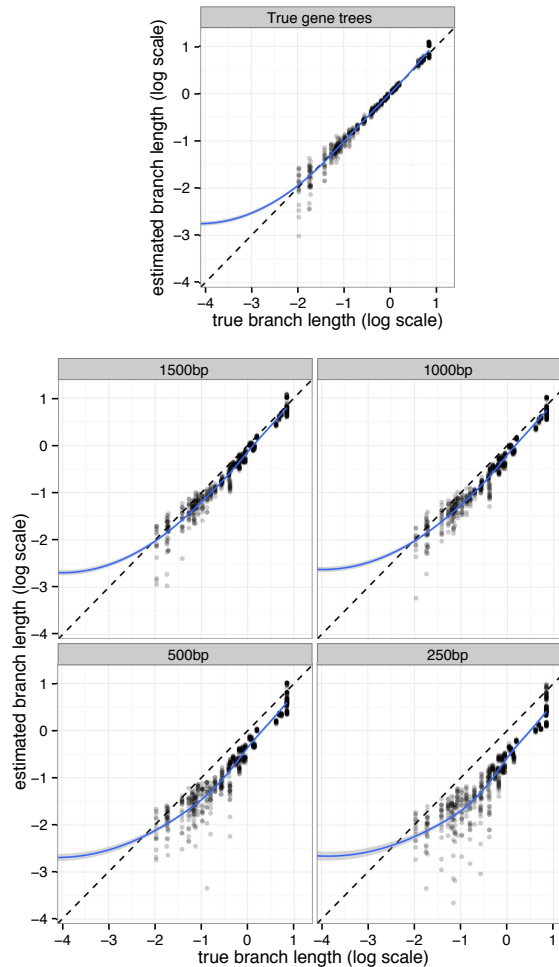


FIG. 6. Branch length accuracy on the avian dataset. Log (base 10) transformed estimated branch lengths are shown versus true branch lengths, and a generalized additive model is fitted to the data. One branch with length $1e-6$ is trimmed out (shown in Fig. S9).

average 3.8 times too short or long. Moreover, unlike true gene trees, the error in branch lengths estimated based on estimated gene trees is biased toward underestimation (Fig. 6), a pattern that increases in intensity with shorter alignments.

Biological datasets

For each biological dataset, we show MLBS support and the local posterior probabilities, computed based on RAxML gene trees available from respective publications. We also collapse gene tree branches with less than 33% bootstrap support, and use these collapsed gene trees to draw local posterior probabilities. For ease of discussion, we show local posterior probabilities as percentages and refer to them simply as posterior or collapsed posterior (for values based on collapsed gene trees). We discuss the confidence in important branches in each tree.

1KP: Three of the key relationships studied by Wickett *et al.* (2014) are the sister branch to land plants, the base of the angiosperms, and the relationship among Bryophytes (hornworts, liverworts, and

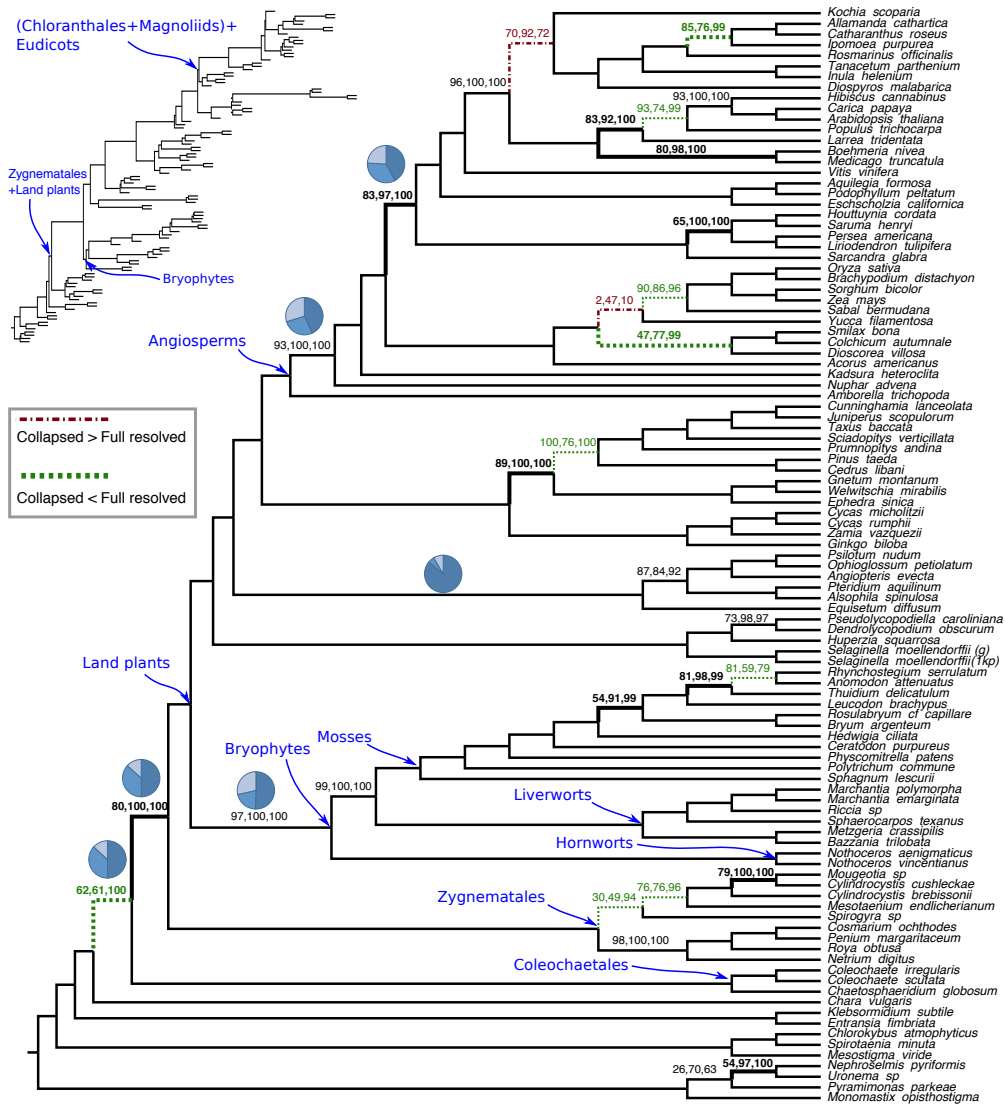


FIG. 7. Support values for the ASTRAL tree on the 1KP dataset of Wickett *et al.* (2014) (103 taxa and 424 genes). On each branch three support values are shown: BS (using site-only MLBS), local posterior computed on fully resolved ML gene trees, and local posterior computed on collapsed ML gene trees (removing branches with <33% BS). Branches with no designation have 100% support with all three measures. Dotted/green lines (dashed/red lines): collapsing low support gene trees branches increases (decreases) posterior by at least 10%. Bold: collapsed posterior is at least 10% higher than BS. Inset: ASTRAL tree with branch lengths in coalescent units shown for internal branches (terminal lengths drawn arbitrarily). Pie-charts (for selected edges): relative frequencies of the three quartet topologies around a branch in collapsed gene trees.

mosses). In the ASTRAL tree, many branches have full support regardless of the measure of the support used, but the remaining branches reveal interesting patterns (Fig. 7). The sister relationship between Zygnetales and land plants receives a moderate 80% BS, but has 100% posterior. Wickett *et al.* (2014) also recovered this relationship by concatenation of various data partitions. There are 12 other branches that have collapsed posteriors that are at least 10% higher than BS (Fig. 7); no branch has substantially higher BS than collapsed posterior. Collapsed posterior for monophyly of Bryophytes and for Amborella as sister to other angiosperms are 100% (compared to 97% and 93% BS, respectively).

When we collapse low support branches in gene trees, posterior goes up for several branches: nine branches have improvements of 10% or more, and only two branches have comparable reductions. An

interesting case is Coleochaetales as sister to Zygnematales+land plants, which has only 62% BS and 61% posterior, but has 100% collapsed posterior. Finally, note that several branches have low posterior, even after collapsing.

Our estimated branch lengths are short for several nodes. For example, the branch that unites (Chloranthales+Magnoliids) and Eudicots has a length of 0.14 in coalescent units. Other branches that have been historically hard to recover also tend to have short branches; however, these are not necessarily extremely short branches that would implicate anomaly zone (two adjacent branches below 0.1 will result in an anomaly zone (Rosenberg, 2013)). For example, Bryophytes had a length of 0.30, and Zygnematales+land plants had a length of 0.28. These values, while short, are not below the often-cited 0.1 threshold. Moreover, as our simulation study showed, we caution that branch lengths tend to be underestimated because of gene tree error and these numbers should be treated as lower bounds.

Angiosperms: Xi *et al.* (2014) have used 310 genes to study the base of the angiosperm tree, a question of intense debate (e.g., Goremykin *et al.*, 2013; Simmons and Gatesy, 2015; Soltis *et al.*, 2011; Zhang *et al.*, 2012). Unlike the MP-EST tree by Xi *et al.* (2014), but similar to concatenation on this dataset and ASTRAL and concatenation on 1KP, the ASTRAL tree recovers Amborella as sister to the rest of the angiosperms. This relationship has 75% BS, but its posterior and collapsed posterior are 100% (Fig. S10). The length of this branch is estimated to be 0.162, almost exactly matching the length estimated on the 1KP dataset (0.158).

Avian (genomes): Jarvis *et al.* (2014) used whole-genomes of 48 bird species to resolve long-standing questions about relationships at the base of Neoaves. We reanalyzed their 2022 supergene trees (binned gene trees; see (Mirarab *et al.*, 2014c)) using ASTRAL, which produced a tree with a wall of short branches at the base of Neoaves (Fig. S11); 12 branches are below 0.1 coalescent units, and another 12 are below 0.5. However, when low support branches in gene trees were collapsed, branch lengths increase by a median of 0.23 units. Nevertheless, 11 branches remain below 0.1, and another four branches are below 0.5. Our results support the hypothesis that avian big bang (Feduccia, 2003) gave rise to very short branches, but quantifying the exact lengths remains difficult because of gene tree error.

Support values on the avian tree also revealed interesting patterns. Despite the large number of supergene trees (2022), which should increase support (Fig. 2), several key branches have low posterior. For example, the position of Hoatzin (arguably, the most difficult avian order to place) and the two branches around it have collapsed posterior below 50% and posterior below 75% (Fig. S11). Similarly, at the base of Neoaves, a clade containing land birds, water birds, and Caprimulgiformes has full support,

but the sister to this large group has only 61% posterior and 80% collapsed posterior. However, other challenging relationships have full support (e.g., falcons as sister to parrots+passerines, and seriema as sister to this group, or a clade containing owls, eagles, and vultures). Thus, despite large number of input trees, posterior probabilities reveal some uncertainty. Finally, on this dataset, unlike the 1KP dataset, four branches have substantially lower posterior compared to BS, and posteriors are higher than collapsed posteriors in some cases.

Avian (high sampling): Prum *et al.* (2015) used their dataset of 259 genes and 201 species to study the avian tree with high taxon sampling. The ASTRAL tree reported by Prum *et al.* (2015) has low MLBS (Fig. S12), and many branches remain poorly supported with posterior probabilities (the median difference between BS and collapsed posterior was 0). Moreover, many of the most interesting relationships are poorly supported. For example, the sister to parrots+passerine has only 30% MLBS support, 83% local posterior support, and 0% collapsed posterior. These low support values are encouraging because the sister to parrots+passerine is likely recovered incorrectly in this tree, as most recent studies put falcons as sister to this group (Jarvis *et al.*, 2014; Kimball *et al.*, 2013; McCormack *et al.*, 2013; Suh *et al.*, 2011). Overall, despite its large taxon sampling, this dataset provides little resolution for the early Neoaves radiation using ASTRAL because of the insufficient gene count for this high level of ILS. Just like the avian genomic data, here we obtain a wall of short branches around the assumed rapid radiation of Neoaves (Fig S12).

Discussions

The local posterior probabilities introduced in this paper can be computed quickly and without a need for extensive MCMC sampling or bootstrapping. Computing posteriors for a species tree with 200 taxa and 1000 genes takes only 10 seconds and for a dataset with 1000 taxa and 1000 genes, takes about three minutes on a laptop machine. This extremely fast computation is possible only because of the two main assumptions of the method: that true MSC-generated gene trees are given and the locality assumption (i.e., the four clusters around each internal branch are present in the true tree). These assumptions can both be violated on real data. Recognizing this fact, our simulations include conditions that violate these two assumptions by introducing plenty of gene tree estimation error (ranging from average RF distance of 25% to 67%) as well as species tree error (Table 1 and Fig. S1).

Our method allows very few false positives with high support, a pattern that is retained even with high levels of gene trees estimation error. It could be argued that our method is perhaps too conservative and underestimates support. Nevertheless, local posterior probabilities were *less* conservative than MLBS,

the only viable alternative for large datasets. Despite allowing very few false positives with high support, the method generally had high recall (i.e., true branches with high support) except for very few genes for a given amount of ILS. Reassuringly, adding gene tree estimation error, while reducing the recall, still retained very high precision. While underestimation of support is not desirable, abundance of false branches with high support would be a more serious problem.

A practical question is what threshold of support should be used to judge a branch reliable. This question is not easy to answer and depends on the false positive rate desired, but also on the amount of gene tree error. Nevertheless, it seems that the commonly used 0.95 threshold results in very high precision while retaining moderately high recall. In our analyses, even lower thresholds (like 0.9 or even 0.7) seemed to give high precision, while increasing the recall.

Gene tree estimation error

Our data revealed an interesting pattern. When gene trees are estimated (but not with true gene trees), at a given threshold, the precision is slightly higher for higher levels of ILS compared to lower ILS (Fig. 3A). We postulate this effect is related to the larger impact that gene tree estimation error has on the total amount of observed discordance for low ILS compared to high ILS conditions (Fig. 8). Consistent with this explanation, we also observed a larger degradation of branch length accuracy in going from true to estimated gene trees for low ILS conditions compared to high ILS (Table 3).

The issue of gene tree estimation error is at the heart of why we saw a need for developing this new method. Sets of site-resampled bootstrap gene trees tend to have increased levels of discordance with regard to the species tree (and also among themselves) compared to ML gene trees, especially when each gene has limited phylogenetic signal. Bootstrapped gene trees have much higher rates of discordance than either true gene trees or ML gene trees (Fig. 8). It is expected that bootstrapped replicates of a dataset result in noisier estimates of parameters than ML; however, the added error by bootstrapping should not be *biased*. For MLBS, the input to the summary method is not just a noisy dataset, but a *biased* one with increased levels of discordance. We postulate this bias is the reason for the underperformance of MLBS.

Our method, on the other hand, does not require bootstrapping and uses the best available gene trees (e.g., estimated ML gene trees). While ML gene trees are still biased towards increased discordance (and hence reduced branch length), they are better than bootstrapped gene trees (Fig 8). The downside of our approach is that gene tree uncertainty is not considered directly. Thus, it was reassuring to see that our method remains precise with high gene tree estimation error. To account for gene tree estimation error, one can collapse the most poorly resolved branches in gene trees when computing support. As we show in our analyses of biological data, this practice seems promising. However, we note that when collapsing

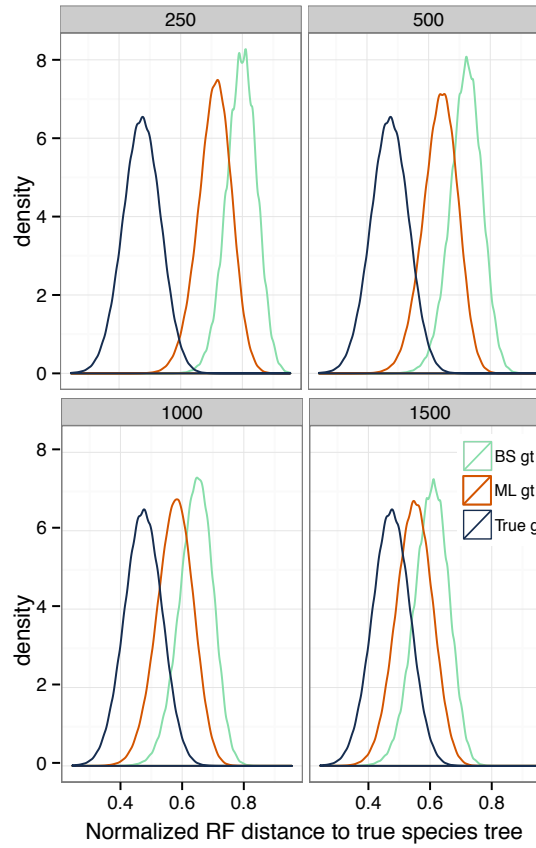


FIG. 8. Gene tree discordance for avian dataset. We show the density plot of the normalized RF distance between the true species tree and true gene trees, ML gene trees, and BS gene trees for four different model conditions.

branches, one should be careful not to introduce bias, which can happen with aggressive filtering. We choose to collapse branches with support below 33% (which can be considered randomly resolved). Future work need to further study the effect of collapsing low support branches in gene trees on both branch length and support.

The impact of gene tree estimation error was most clear with estimates of the branch length. The branch lengths produced by this method showed encouraging patterns (e.g., consistency across biological datasets); nevertheless, our estimated branch lengths are not immune to underestimation that is seen often with other summary methods. Thus, we suggest branch lengths from ASTRAL and other summary methods should be interpreted with care in the presence of gene tree estimation error.

High support despite high discordance

An important observation, predicted by the theory but sometimes lost in the scientific debate about discordance, is that high confidence for a correctly inferred relationship can emerge even with high levels of discordance. As Figure 2 shows, a branch that appears in only 40% of gene trees can still be resolved with high confidence if a sufficient number of genes are available (e.g., around 500). For example, in the 1KP tree, the branch that puts Zygnetatales as sister to land plants appeared in only 49% of

collapsed gene trees and the branch making Bryophytes monophyletic only appeared in 50% of them; both branches, however, have a posterior of 1.0. We have implemented an option in ASTRAL to output the percentage of gene tree quartets that agree with each of the three resolutions around a branch. Pie charts in Figure 7 give examples of these relative quartet frequencies.

A question that biologists often face is the number of genes required to resolve a branch. The number of genes required to obtain high resolution and low false positive rates depends on the model condition. With higher ILS, more genes are required, an observation that is not surprising. However, our method can be extended to estimate the number of genes that might be required to resolve a tree (with an estimated level of ILS).

Limitations and future work

Promising approaches for incorporating gene tree uncertainty into local posterior probabilities exist. For example, one can weight each gene tree quartet around a branch by its SH-like support, BS, or advanced measures like concordance (Ané *et al.*, 2007). Moreover, comparing our method against Bayesian co-estimation methods on small datasets where they can run will be interesting. Furthermore, we did not investigate the impact of changing prior parameters (λ); nor did we explore other forms prior functions, such as Dirichlet distributions (conjugate to multinomial) or birth-death processes. We leave these for future work.

We violated some but not all assumptions of our method in the experimental results. The sequence evolution models used for simulation and inference were both GTR+ Γ , but on real data, model violations (e.g., compositional bias) can lead to biased estimates of gene trees. Finally, all our simulated datasets had discordance that was generated only by ILS and estimation error, and not other sources of true biological discordance, such as undetected paralogy or horizontal gene transfer. Future work should further examine the impact of other biological sources of discordance on the reliability of local posterior probabilities.

References

Allman, E. S., Degnan, J. H., and Rhodes, J. A. 2011. Identifying the rooted species tree from the distribution of unrooted gene trees under the coalescent. *J. Math. Biol.*, 62: 833–862.

Andrade, S. C. S., Novo, M., Kawauchi, G. Y., Worsaae, K., Pleijel, F., Giribet, G., and Rouse, G. W. 2015. Articulating archiannelids: Phylogenomics and annelid relationships, with emphasis on meiofaunal taxa. *Molecular Biology and Evolution*.

Ané, C., Larget, B. R., Baum, D. A., Smith, S. D., and Rokas, A. 2007. Bayesian estimation of concordance among gene trees. *Molecular Biology and Evolution*, 24(2): 412–426.

Bayzid, M. S., Mirarab, S., Boussau, B., and Warnow, T. 2015. Weighted Statistical Binning: Enabling Statistically Consistent Genome-Scale Phylogenetic Analyses. *PLoS ONE*, 10(6): e0129183.

Bryant, D., Bouckaert, R., Felsenstein, J., Rosenberg, N. A., and Roychoudhury, A. 2012. Inferring species trees directly from biallelic genetic markers: Bypassing gene trees in a full coalescent analysis. *Molecular Biology and Evolution*, 29(8): 1917–1932.

Chifman, J. and Kubatko, L. S. 2014. Quartet Inference from SNP Data Under the Coalescent Model. *Bioinformatics*, 30(23): 3317–3324.

Degnan, J. H. 2013. Anomalous unrooted gene trees. *Systematic Biology*, 62: 574–590.

Degnan, J. H. and Rosenberg, N. A. 2006. Discordance of Species Trees with Their Most Likely Gene Trees. *PLoS Genet*, 2(5).

Feduccia, A. 2003. 'Big bang' for tertiary birds?

Felsenstein, J. 1985. Confidence Limits on Phylogenies: An Approach Using the Bootstrap. *Evolution*, 39(4): 783–791.

Felsenstein, J. and Kishino, H. 1993. Is there something wrong with the bootstrap on phylogenies? A reply to Hillis and Bull. *Systematic Biology*, 42(2): 193–200.

Gatesy, J. and Springer, M. S. 2014. Phylogenetic Analysis at Deep Timescales: Unreliable Gene Trees, Bypassed Hidden Support, and the Coalescence/Concatalescence Conundrum. *Molecular phylogenetics and evolution*, 80: 231–266.

Giarla, T. C. and Esselstyn, J. A. 2015. The Challenges of Resolving a Rapid, Recent Radiation: Empirical and Simulated Phylogenomics of Philippine Shrews. *Systematic biology*, page syv029.

Goremykin, V. V., Nikiforova, S. V., Biggs, P. J., Zhong, B., Delange, P., Martin, W., Woetzel, S., Atherton, R. A., McLenaghan, P. A., and Lockhart, P. J. 2013. The Evolutionary Root of Flowering Plants. *Systematic Biology*, 62(1): 50–61.

Grover, C. E., Gallagher, J. P., Jareczek, J. J., Page, J. T., Udall, J. A., Gore, M. A., and Wendel, J. F. 2015. Re-evaluating the phylogeny of allopolyploid *Gossypium* L. *Molecular phylogenetics and evolution*.

Guindon, S., Delsuc, F., Dufayard, J. F., and Gascuel, O. 2009. Estimating maximum likelihood phylogenies with PhyML. *Methods in Molecular Biology*, 537: 113–137.

Heled, J. and Drummond, A. J. 2010. Bayesian inference of species trees from multilocus data. *Molecular Biology and Evolution*, 27(3): 570–580.

Hillis, D. M. and Bull, J. J. 1993. An Empirical Test of Bootstrapping as a Method for Assessing Confidence in Phylogenetic Analysis. *Systematic Biology*, 42(2): 182–192.

Hoschek, W. 2002. The Colt distribution: Open source libraries for high performance scientific and technical computing in JAVA. *URL: http://nicewww. cern. ch/hoschek/colt/index. htm.*

Hosner, P. A., Faircloth, B. C., Glenn, T. C., Braun, E. L., and Kimball, R. T. 2011. Avoiding missing data biases in phylogenomic inference: an empirical study in the landfowl (Aves: Galliformes). *Molecular biology and evolution*, (785): 1–12.

Jarvis, E. D., Mirarab, S., Aberer, A. J., Li, B., Houde, P., Li, C., Ho, S. Y. W., Faircloth, B. C., Nabholz, B., Howard, J. T., Suh, A., Weber, C. C., da Fonseca, R. R., Li, J., Zhang, F., Li, H., Zhou, L., Narula, N., Liu, L., Ganapathy, G., Boussau, B., Bayzid, M. S., Zavidovych, V., Subramanian, S., Gabaldón, T., Capella-Gutiérrez, S., Huerta-Cepas, J., Rekepalli, B., Munch, K., Schierup, M. H., Lindow, B., Warren, W. C., Ray, D., Green, R. E., Bruford, M. W., Zhan, X., Dixon, A., Li, S., Li, N., Huang, Y., Derryberry, E. P., Bertelsen, M. F., Sheldon, F. H., Brumfield, R. T., Mello, C. V., Lovell, P. V., Wirthlin, M., Schneider, M. P. C., Prosdocimi, F., Samaniego, J. A., Velazquez, A. M. V., Alfaro-Núñez, A., Campos, P. F., Petersen, B., Sicheritz-Ponten, T., Pas, A., Bailey, T., Scofield, P., Bunce, M., Lambert, D. M., Zhou, Q., Perelman, P., Driskell, A. C., Shapiro, B., Xiong, Z., Zeng, Y., Liu, S., Li, Z., Liu, B., Wu, K., Xiao, J., Yinqi, X., Zheng, Q., Zhang, Y., Yang, H., Wang, J., Smeds, L., Rheindt, F. E., Braun, M. J., Fjeldsa, J., Orlando, L., Barker, F. K., Jönsson, K. A., Johnson, W., Koepfli, K.-P., O'Brien, S., Haussler, D., Ryder, O. A., Rahbek, C., Willerslev, E., Graves, G. R., Glenn, T. C., McCormack, J. E., Burt, D. W., Ellegren, H., Alström, P., Edwards, S. V., Stamatakis, A., Mindell, D. P., Cracraft, J., Braun, E. L., Warnow, T., Jun, W., Gilbert, M. T. P., and Zhang, G. 2014. Whole-genome analyses resolve early branches in the tree of life of modern birds. *Science*, 346(6215): 1320–1331.

Kimball, R. T., Wang, N., Heimer-McGinn, V., Ferguson, C., and Braun, E. L. 2013. Identifying localized biases in large datasets: a case study using the avian tree of life. *Molecular phylogenetics and evolution*, 69(3): 1021–32.

Kubatko, L. S. and Degnan, J. H. 2007. Inconsistency of phylogenetic estimates from concatenated data under coalescence. *Systematic Biology*, 56: 17–24.

Larget, B. R., Kotha, S. K., Dewey, C. N., and Ané, C. 2010. BUCKy: gene tree/species tree reconciliation with Bayesian concordance analysis. *Bioinformatics*, 26(22): 2910–2911.

Laumer, C. E., Hejnol, A., and Giribet, G. 2015. Nuclear genomic signals of the 'microturbellarian' roots of platyhelminth evolutionary innovation. *eLife*, 4.

Liu, L. 2008. BEST: Bayesian estimation of species trees under the coalescent model. *Bioinformatics (Oxford, England)*, 24(21): 2542–2543.

Liu, L. and Yu, L. 2011. Estimating species trees from unrooted gene trees. *Systematic Biology*, 60: 661–667.

Liu, L., Yu, L., Pearl, D. K., and Edwards, S. V. 2009. Estimating species phylogenies using coalescence times among sequences. *Systematic Biology*, 58(5): 468–477.

Liu, L., Yu, L., and Edwards, S. V. 2010. A maximum pseudo-likelihood approach for estimating species trees under the coalescent model. *BMC Evolutionary Biology*, 10(1): 302.

Maddison, W. P. 1997. Gene Trees in Species Trees. *Systematic Biology*, 46(3): 523–536.

Mallo, D., Martins, L. d. O., and Posada, D. 2015. SimPhy : Phylogenomic Simulation of Gene , Locus and Species Trees. *Syst. Biol.*

McCormack, J. E., Harvey, M. G., Faircloth, B. C., Crawford, N. G., Glenn, T. C., and Brumfield, R. T. 2013. A Phylogeny of Birds Based on Over 1,500 Loci Collected by Target Enrichment and High-Throughput Sequencing. *PLoS ONE*, 8(1): e54848.

Mirarab, S. and Warnow, T. 2015. ASTRAL-II: coalescent-based species tree estimation with many hundreds of taxa and thousands of genes. *Bioinformatics*, 31(12): i44–i52.

Mirarab, S., Reaz, R., Bayzid, M. S., Zimmermann, T., Swenson, M. S., and Warnow, T. 2014a. ASTRAL: genome-scale coalescent-based species tree estimation. *Bioinformatics*, 30(17): i541–i548.

Mirarab, S., Bayzid, M. S., and Warnow, T. 2014b. Evaluating summary methods for multi-locus species tree estimation in the presence of incomplete lineage sorting. *Systematic Biology*, page syu063.

Mirarab, S., Bayzid, M. S., Boussau, B., and Warnow, T. 2014c. Statistical binning enables an accurate coalescent-based estimation of the avian tree. *Science*, 346(6215): 1250463–1250463.

Mossel, E. and Roch, S. 2010. Incomplete lineage sorting: consistent phylogeny estimation from multiple loci. *IEEE/ACM Transactions on Computational Biology and Bioinformatics*, 7(1): 166–171.

Nguyen, N., Mirarab, S., and Warnow, T. 2012. MRL and SuperFine+ MRL: new supertree methods. *Algorithms for Molecular Biology*, 7(1): 3.

Price, M. N., Dehal, P. S., and Arkin, A. P. 2010. FastTree-2 Approximately Maximum-Likelihood Trees for Large Alignments. *PLoS ONE*, 5(3): e9490.

Prum, R. O., Berv, J. S., Dornburg, A., Field, D. J., Townsend, J. P., Lemmon, E. M., and Lemmon, A. R. 2015. A comprehensive phylogeny of birds (Aves) using targeted next-generation DNA sequencing. *Nature*, advance on.

Ragan, M. a. 1992. Phylogenetic inference based on matrix representation of trees. *Molecular Phylogenetics and Evolution*, 1(1): 53–58.

Rannala, B. and Yang, Z. 2003. Bayes estimation of species divergence times and ancestral population sizes using DNA sequences from multiple loci. *Genetics*, 164(4): 1645–1656.

Robinson, D. and Foulds, L. 1981. Comparison of phylogenetic trees. *Mathematical Biosciences*, 53(1-2): 131–147.

Roch, S. and Steel, M. 2014. Likelihood-based tree reconstruction on a concatenation of aligned sequence data sets can be statistically inconsistent. *Theoretical population biology*, 100: 56–62.

Rosenberg, N. A. 2013. Discordance of species trees with their most likely gene trees: a unifying principle. *Molecular Biology and Evolution*, 30(12): 2709–2713.

Salichos, L. and Rokas, A. 2013. Inferring ancient divergences requires genes with strong phylogenetic signals. *Nature*, 497(7449): 327–31.

Seo, T.-K. 2008. Calculating Bootstrap Probabilities of Phylogeny Using Multilocus Sequence Data. *Molecular Biology and Evolution*, 25(5): 960–971.

Seo, T.-K., Kishino, H., and Thorne, J. L. 2005. Incorporating gene-specific variation when inferring and evaluating optimal evolutionary tree topologies from multilocus sequence data. *Proc Natl Acad Sci USA*, 102(12): 4436–41.

Simmons, M. P. and Gatesy, J. 2015. Coalescence vs. concatenation: sophisticated analyses vs. first principles applied to rooting the angiosperms. *Molecular phylogenetics and evolution*.

Soltis, D. E., Smith, S. A., Cellinese, N., Wurdack, K. J., Tank, D. C., Brockington, S. F., Refulio-Rodriguez, N. F., Walker, J. B., Moore, M. J., Carlsward, B. S., Bell, C. D., Latvis, M., Crawley, S., Black, C., Diouf, D., Xi, Z., Rushworth, C. A., Gitzendanner, M. A., Sytsma, K. J., Qiu, Y., Hilu, K. W., Davis, C. C., Sanderson, M. J., Beaman, R. S., Olmstead, R. G., Judd, W. S., Donoghue, M. J., and Soltis, P. S. 2011. Angiosperm phylogeny: 17 genes, 640 taxa. *American Journal of Botany*, 98: 704–730.

Song, S., Liu, L., Edwards, S. V., and Wu, S. 2012. Resolving conflict in eutherian mammal phylogenomics and the multispecies coalescent model. *Proceedings of the National Academy of Sciences of the United States of America*, 109(37): 14942–7.

Stadler, T. and Steel, M. 2012. Distribution of branch lengths and phylogenetic diversity under homogeneous speciation models. *Journal of Theoretical Biology*, 297: 33–40.

Stamatakis, A. 2014. RAxML version 8: A tool for phylogenetic analysis and post-analysis of large phylogenies. *Bioinformatics*, 30(9): 1312–1313.

Streicher, J. W., Schulte, J. A., and Wiens, J. J. 2015. How Should Genes and Taxa be Sampled for Phylogenomic Analyses with Missing Data? An Empirical Study in Iguanian Lizards. *Systematic Biology*.

Suh, A., Paus, M., Kieffmann, M., Churakov, G., Franke, F. A., Brosius, J., Kriegs, J. O., and Schmitz, J. 2011. Mesozoic retrotransposons reveal parrots as the closest living relatives of passerine birds. *Nature communications*, 2: 443.

Susko, E. 2009. Bootstrap support is not first-order correct. *Systematic Biology*, 58(2): 211–223.

Vachaspati, P. and Warnow, T. 2015. ASTRID: Accurate Species TRees from Internode Distances. *BMC Genomics*, 16(Suppl 10): S3.

Wickett, N. J., Mirarab, S., Nguyen, N., Warnow, T., Carpenter, E. J., Matasci, N., Ayyampalayam, S., Barker, M. S., Burleigh, J. G., Gitzendanner, M. A., Ruhfel, B. R., Wafula, E., Der, J. P., Graham, S. W., Mathews, S., Melkonian, M., Soltis, D. E., Soltis, P. S., Miles, N. W., Rothfels, C. J., Pokorny, L., Shaw, A. J., DeGironimo, L., Stevenson, D. W., Surek, B., Villarreal, J. C., Roure, B., Philippe, H., DePamphilis, C. W., Chen, T., Deyholos, M. K., Baucom, R. S., Kutchan, T. M., Augustin, M. M., Wang, J., Zhang, Y., Tian, Z., Yan, Z., Wu, X., Sun, X., Wong, G. K.-S., and Leebens-Mack, J. 2014. Phylotranscriptomic analysis of the origin and early diversification of land plants. *Proceedings of the National Academy of Sciences*, 111(45): E4859–4868.

Wood, S. N. 2011. Fast stable restricted maximum likelihood and marginal likelihood estimation of semiparametric generalized linear models. *Journal of the Royal Statistical Society: Series B (Statistical Methodology)*, 73(1): 3–36.

Xi, Z., Liu, L., Rest, J. S., and Davis, C. C. 2014. Coalescent versus Concatenation Methods and the Placement of Amborella as Sister to Water Lilies. *Systematic Biology*, 63(6): 919–932.

Zhang, N., Zeng, L., Shan, H., and Ma, H. 2012. Highly conserved low-copy nuclear genes as effective markers for phylogenetic analyses in angiosperms. *New Phytologist*, 195: 923–937.

Supplementary Material for “Fast coalescent-based computation of local branch support from quartet frequencies”

Erfan Sayyari¹ and Siavash Mirarab^{*1}

¹University of California, San Diego, Department of Electrical and Computer Engineering

Contents

1	Supplementary Figures and Tables	2
2	Supplementary methods	16
3	Proofs	16
3.1	Proof of Lemma 1	16
3.2	Proof of Theorem 1	16
3.3	Proof of Theorem 2	18
3.4	Proof of Lemma 2	19
4	Commands and version numbers	19

List of Figures

S1	Properties of the A-200 dataset.	3
S2	Accuracy of local posterior probability on the A-200 dataset with true species trees.	4
S3	Accuracy of local posterior probability on the A-200 dataset with NJST species trees.	5
S4	Accuracy of local posterior probability on the A-200 dataset with concatenation.	6
S5	Precision of local posterior probability on the Avian dataset with ASTRAL.	7
S6	Recall of local posterior probability on the Avian dataset with ASTRAL.	8
S7	Branch length accuracy on the A-200 Low ILS dataset.	9
S8	Branch length accuracy on the A-200 High ILS dataset.	9
S9	Branch length accuracy on the Avian dataset.	10
S10	Support on the angiosperm dataset	11
S11	Support on the avian dataset	12
S12	Support on the avian dataset of Prum et al.	13
S13	Frequency calculation algorithm.	14
S14	Topologies of different quartets around a branch might heavily depend on each other	15

List of Tables

S1	Support accuracy on the avian dataset.	2
----	--	---

*Corresponding author: smirarab@ucsd.edu

1 Supplementary Figures and Tables

Table S1: **Support accuracy on the avian dataset.** Accuracy (and recall) of BS and local posterior probability is show for three thresholds: 0.7, 0.95, and 0.99.

sites	BS			Local PP with Estimated gene trees			Local PP with True gene trees		
	0.70	0.95	0.99	0.70	0.9	0.99	0.70	0.95	0.99
1500	99.4(93.5)	100.0(89.6)	100.0(85.9)	99.9(90.7)	100.0(84.7)	100.0(81.3)	99.9(93.6)	100.0(90.2)	100.0(86.2)
1000	99.6(89.0)	100.0(79.7)	100.0(74.3)	100.0(91.4)	100.0(84.1)	100.0(80.1)	100.0(94.5)	100.0(91.4)	100.0(87.7)
500	98.0(75.7)	99.8(69.8)	100.0(66.8)	99.5(87.7)	99.8(79.8)	100.0(74.4)	99.0(97.4)	99.4(93.8)	99.5(90.6)
250	95.9(71.7)	99.6(63.2)	100.0(57.4)	99.1(78.3)	100.0(71.5)	100.0(69.2)	97.1(97.7)	98.6(94.7)	99.2(92.6)

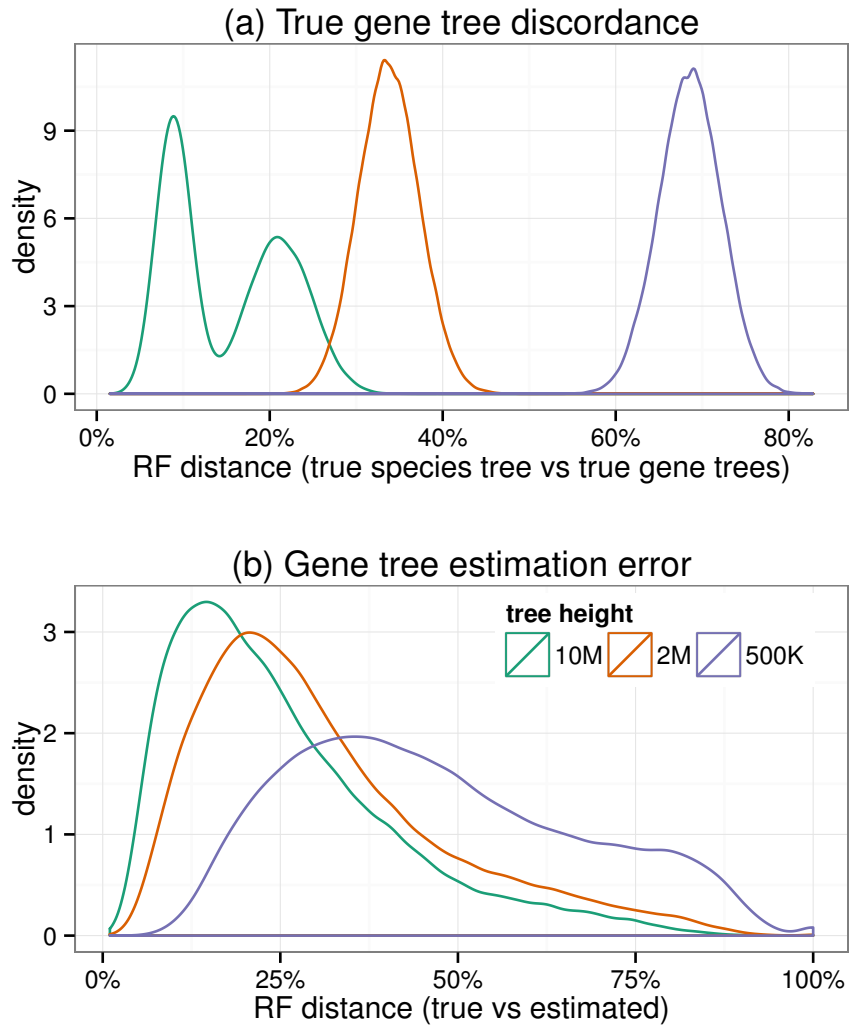
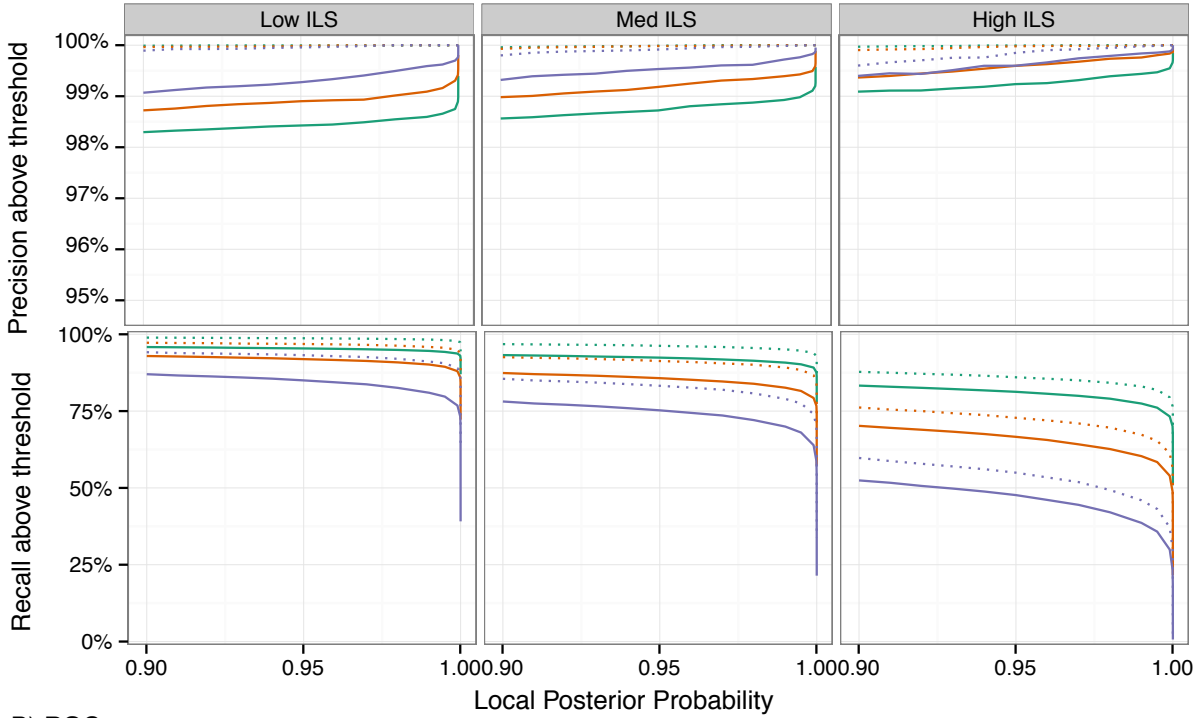


Figure S1: **Properties of the A-200 dataset.** (a) True gene tree discordance is shown, measured as the RF distance [1] between the true species tree and the true gene trees; Three levels of ILS are created by changing tree length (10M, 2M, or 500K generations), resulting in low, medium, and high discordance. The double pick is due to the fact that in [2] two different speciation rates are used, but here, we combine both speciation rates into one larger dataset. Bottom: Gene tree estimation error, measured as the RF distance between the true gene tree and the estimated gene tree. Note that the datasets with higher ILS also tend to have higher gene tree error.

A) Precision and recall



B) ROC

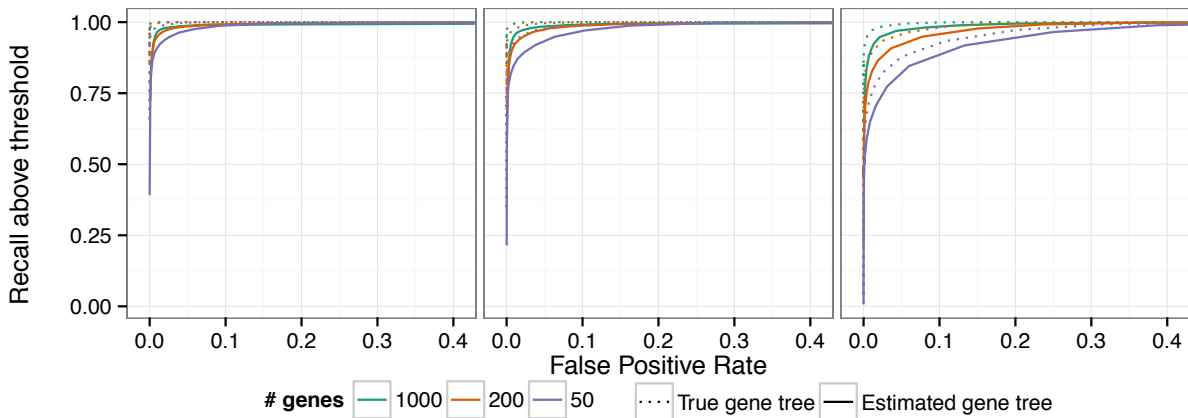
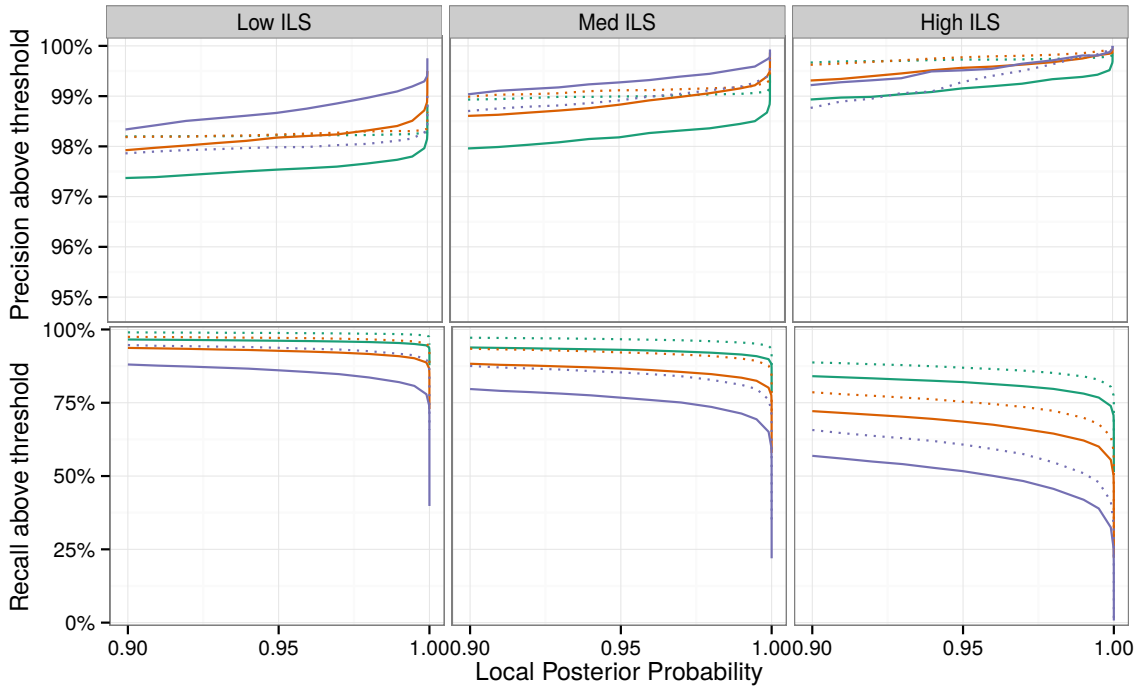


Figure S2: **Accuracy of local posterior probability on the A-200 dataset with true species trees.** A) the precision and recall of branches with local posterior probability above a threshold ranging from 0.9 to 1.0 using estimated gene trees (solid) or true gene trees (dotted). B) ROC curve (recall versus false positive rate) for thresholds ranging from 0 to 1 (figure trimmed at 0.4 fpr). Columns show different levels of ILS (each with 100 replicates). For each branch in each true species tree, all three alternatives are included in the analysis (one correct branch and two wrong branches). Thus, a total of $198*3*100=59400$ branches are included for each model condition.

A) Precision and recall



B) ROC

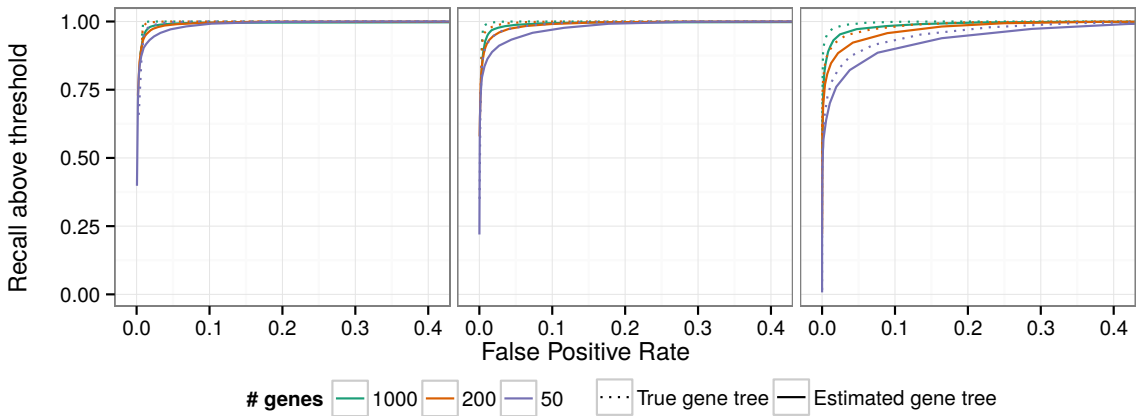
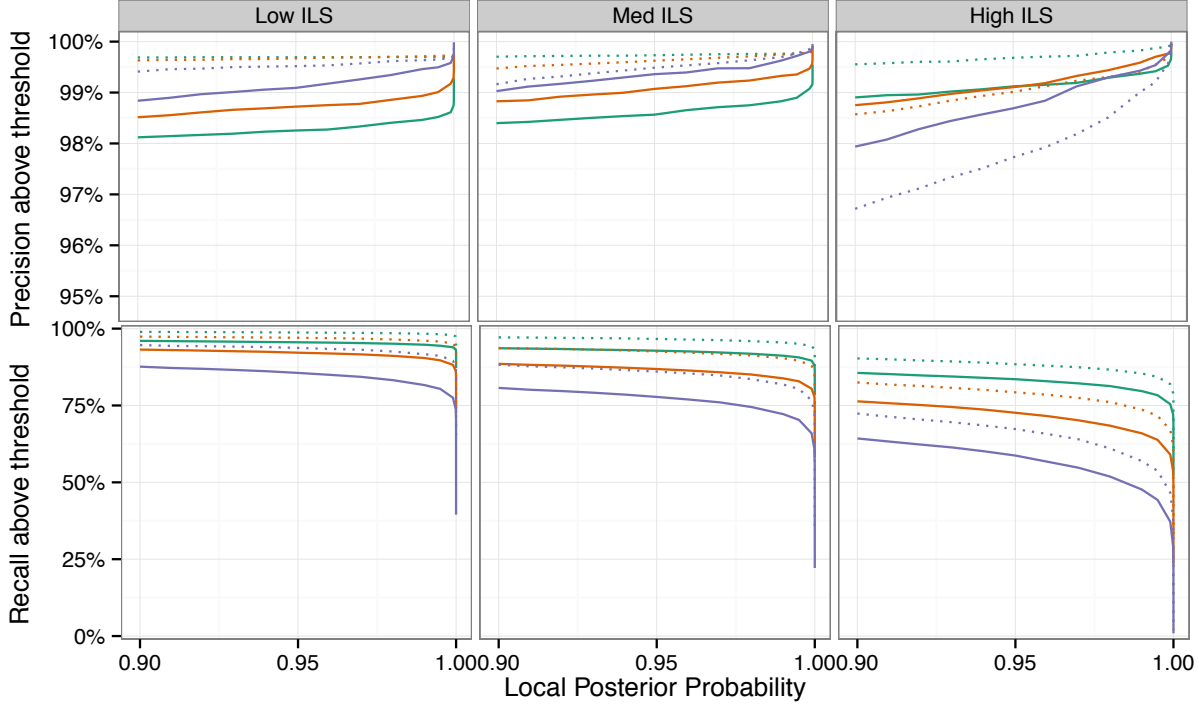


Figure S3: **Accuracy of local posterior probability on the A-200 dataset with NJST species trees.** A) the precision and recall of branches with local posterior probability above a threshold ranging from 0.9 to 1.0 using estimated gene trees (solid) or true gene trees (dotted). B) ROC curve (recall versus false positive rate) for thresholds ranging from 0 to 1 (figure trimmed at 0.4 fpr). Columns show different levels of ILS (each with 100 replicates). For each branch in each true species tree, all three alternatives are included in the analysis (one correct branch and two wrong branches). Thus, a total of $198*3*100=59400$ branches are included for each model condition.

A) Precision and recall



B) ROC

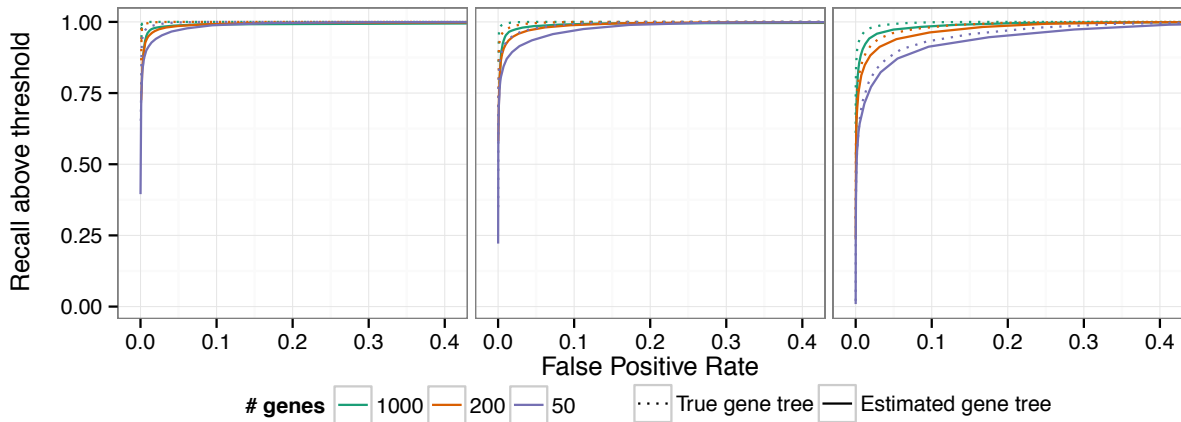


Figure S4: **Accuracy of local posterior probability on the A-200 dataset with concatenation.** A) the precision and recall of branches with local posterior probability above a threshold ranging from 0.9 to 1.0 using estimated gene trees (solid) or true gene trees (dotted). B) ROC curve (recall versus false positive rate) for thresholds ranging from 0 to 1 (figure trimmed at 0.4 fpr). Columns show different levels of ILS (each with 100 replicates). For each branch in each true species tree, all three alternatives are included in the analysis (one correct branch and two wrong branches). Thus, a total of $198*3*100=59400$ branches are included for each model condition.

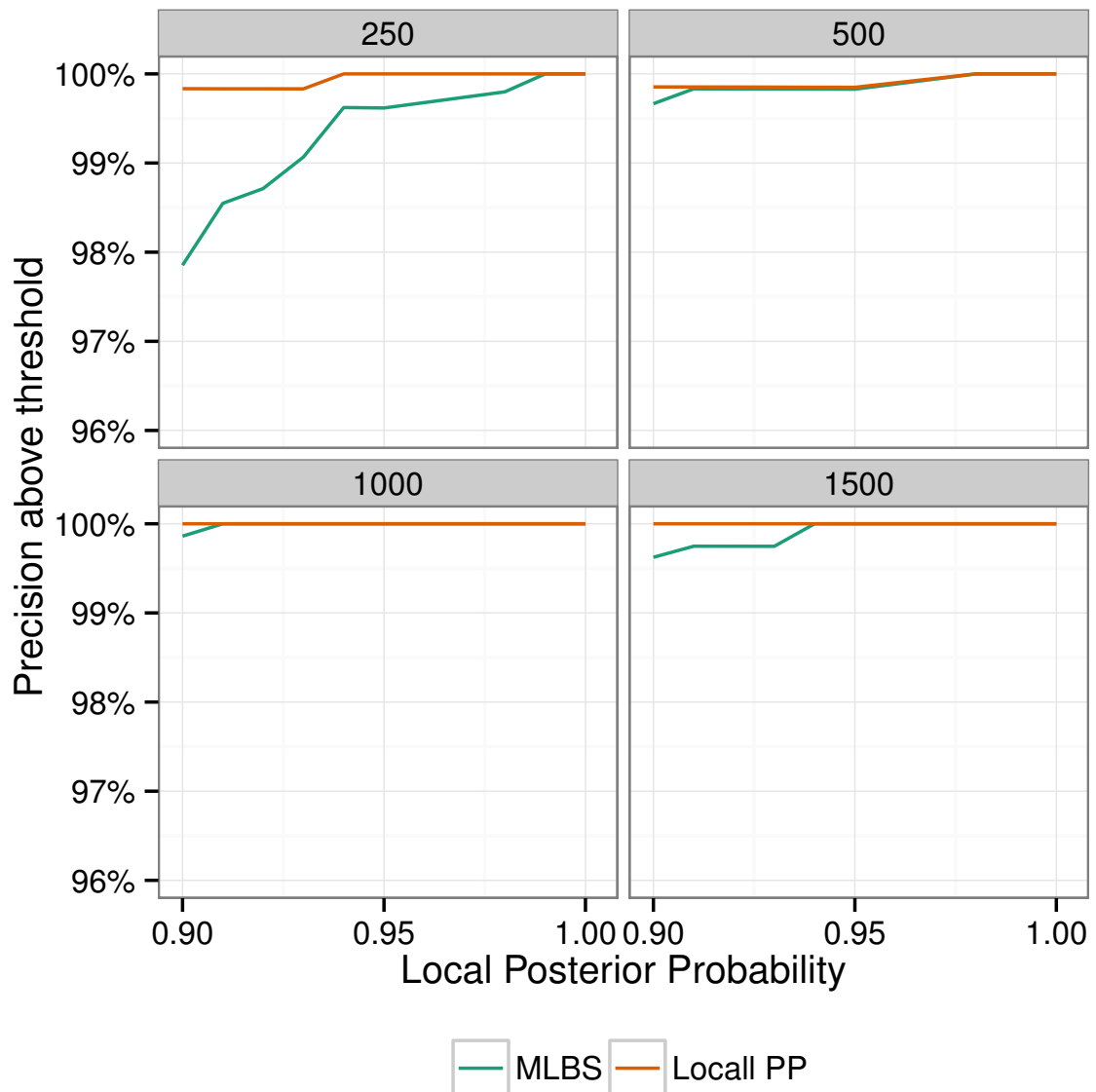


Figure S5: **Precision of local posterior probability on the Avian dataset with ASTRAL.** Precision of branches with local posterior probability above a threshold ranging from 0.9 to 1.0 based on MLBS and local posterior probability (PP) support values. Boxes show different numbers of sites per gene (controlling gene tree estimation error).

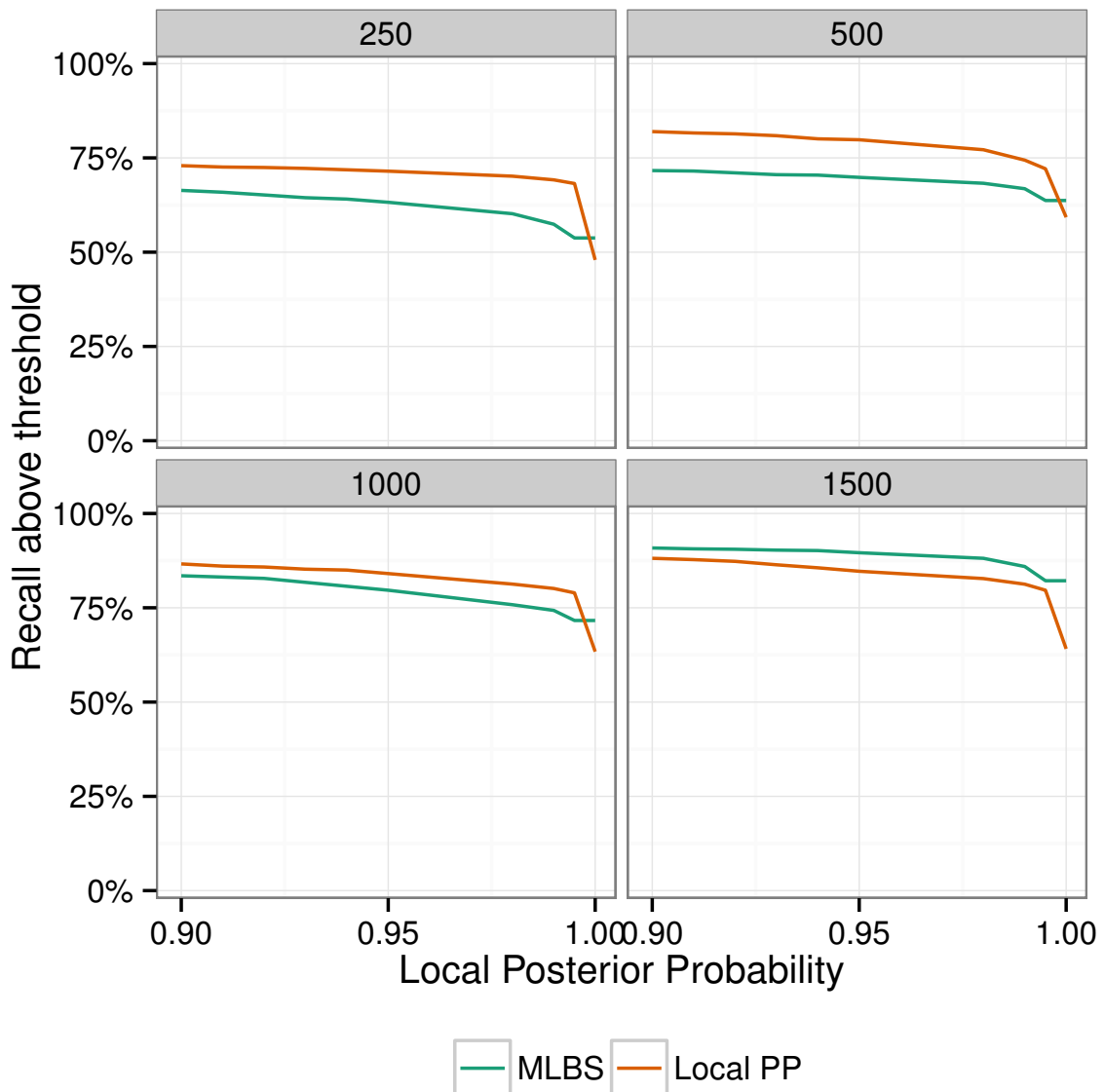


Figure S6: **Recall of local posterior probability on the Avian dataset with ASTRAL.** Recall of branches with local posterior probability above a threshold ranging from 0.9 to 1.0 based on MLBS and local posterior probability (PP) support values. Boxes show different numbers of sites per gene (controlling gene tree estimation error).

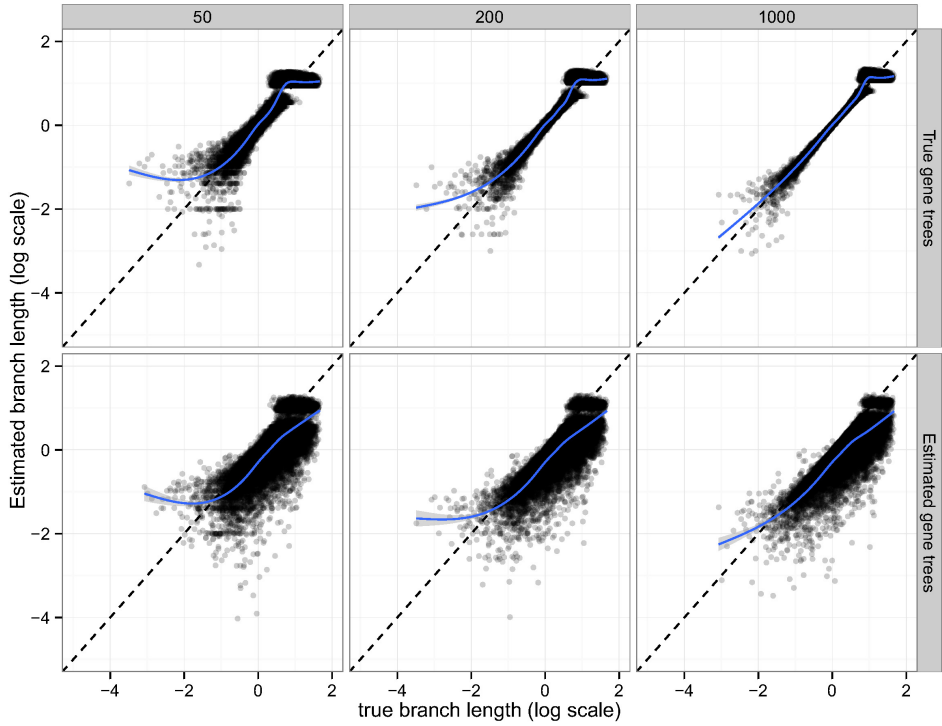


Figure S7: **Branch length accuracy on the A-200 Low ILS dataset.** Estimated branch length is plotted against true branch length in log scale (base 10).

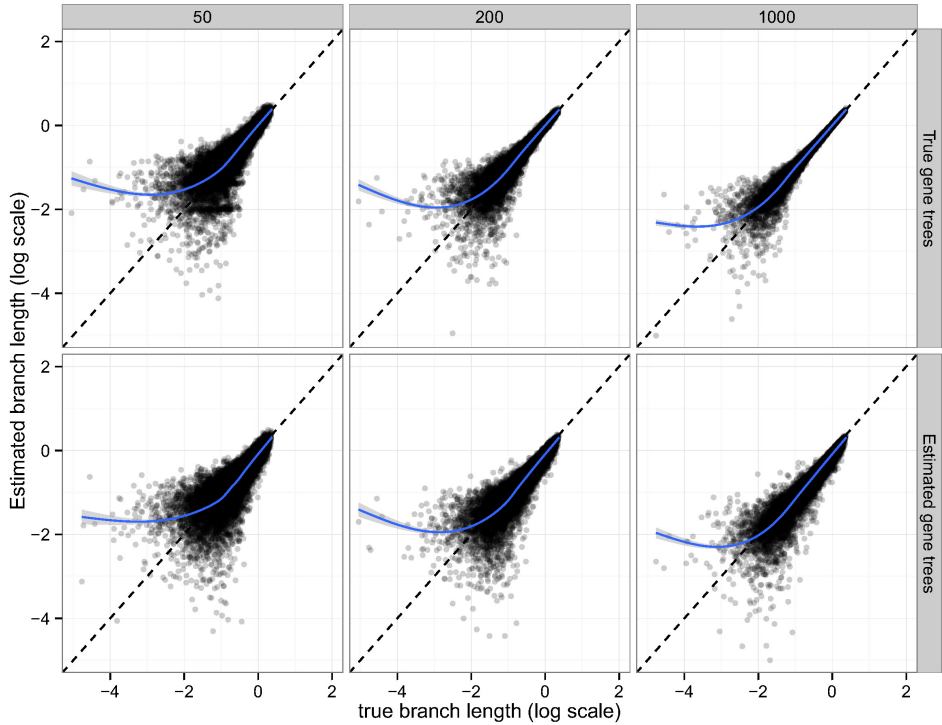


Figure S8: **Branch length accuracy on the A-200 High ILS dataset.** Estimated branch length is plotted against true branch length in log scale (base 10).

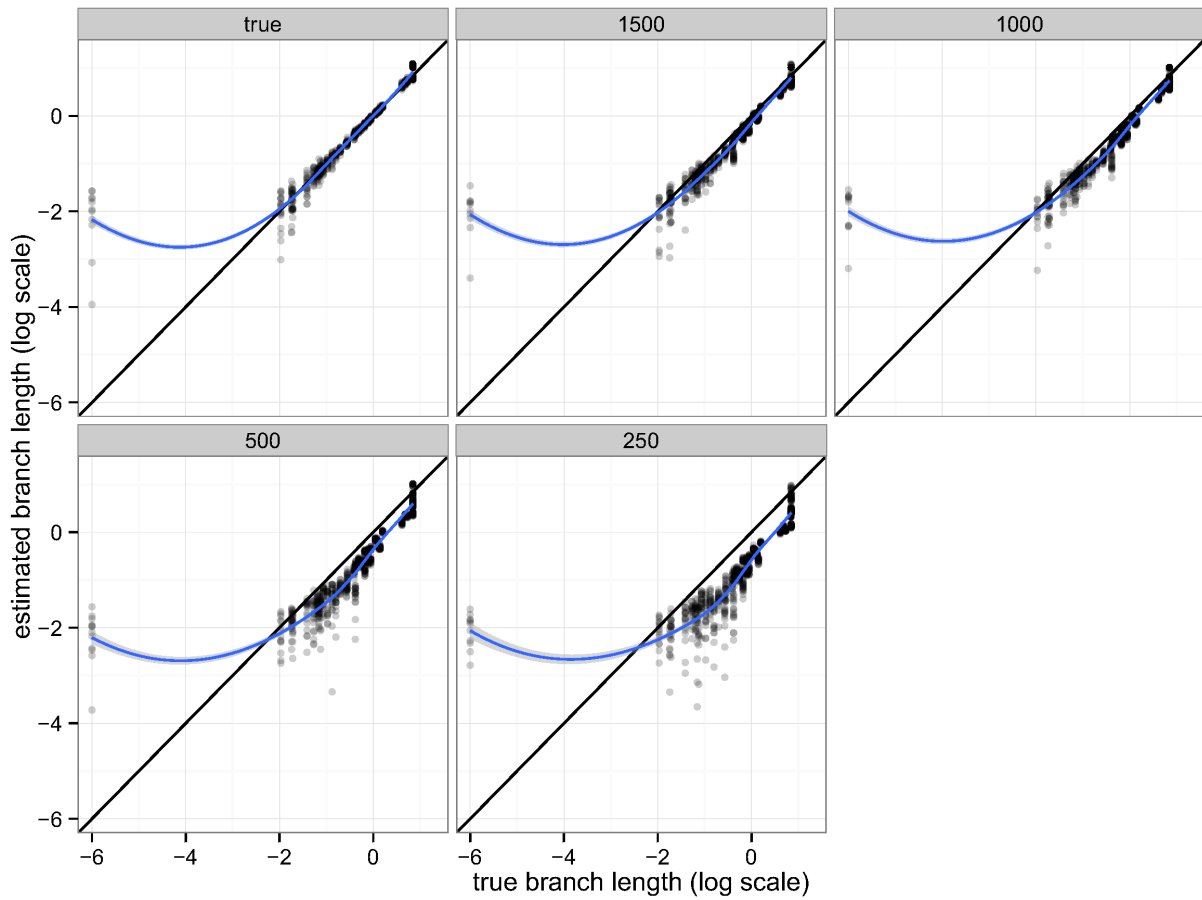


Figure S9: **Branch length accuracy on the Avian dataset.** Estimated branch length is plotted against true branch length in log scale (base 10).

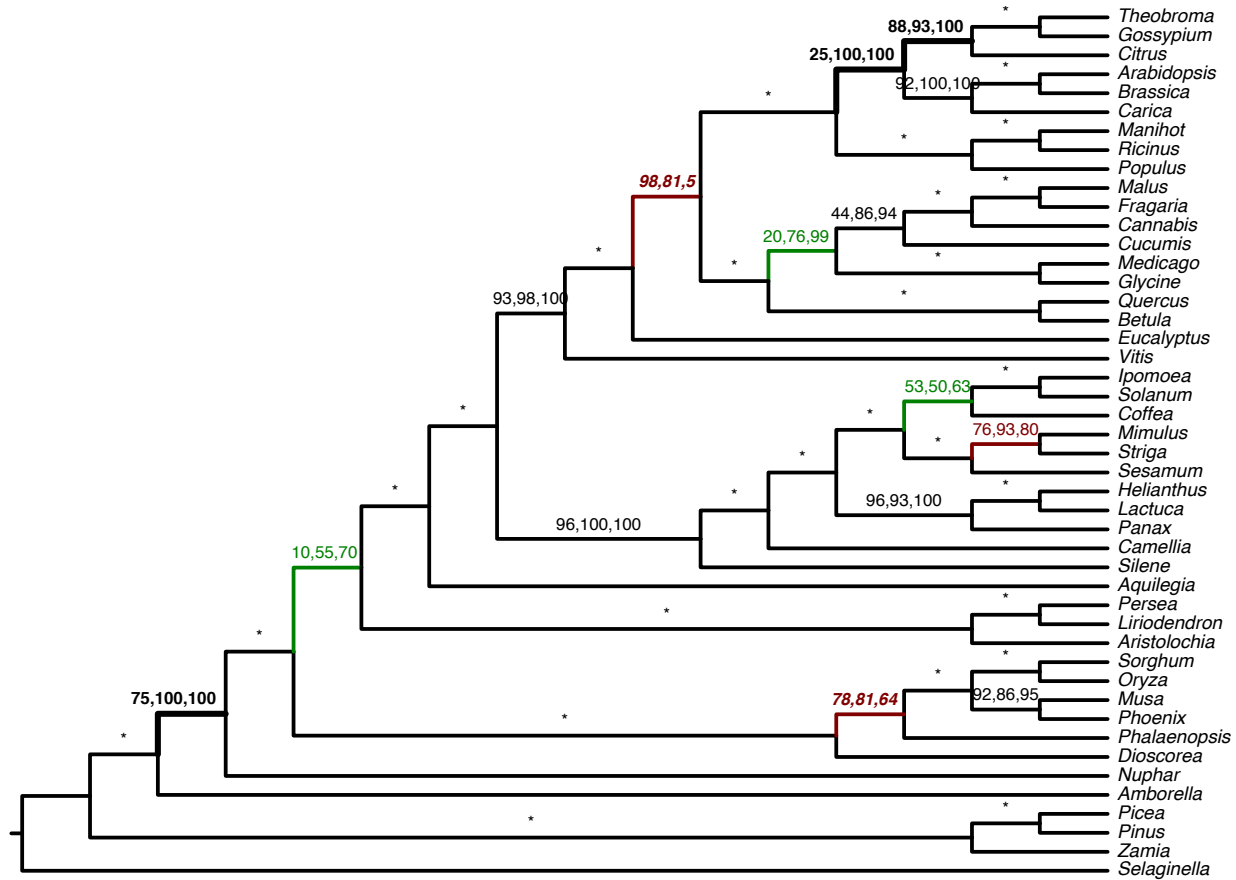


Figure S10: **Support on the angiosperm dataset** Three forms of support values are shown for the angiosperm dataset of Xi et al [3]. MLBS support (site-only), local posterior computed on fully ML resolved gene trees, and local posterior computed on ML gene trees with branches with less than 33% support collapsed. Branches marked with an asterisk (*) have 100% support with all three measures. Bold: local support on collapsed gene trees is at least 10% higher than MLBS support. Bold italic: local support on collapsed gene trees is at least 10% lower than MLBS support. Dotted/green lines (dashed/red lines): collapsing low support branches in gene trees increases (decreases) local posterior probability by at least 10%.

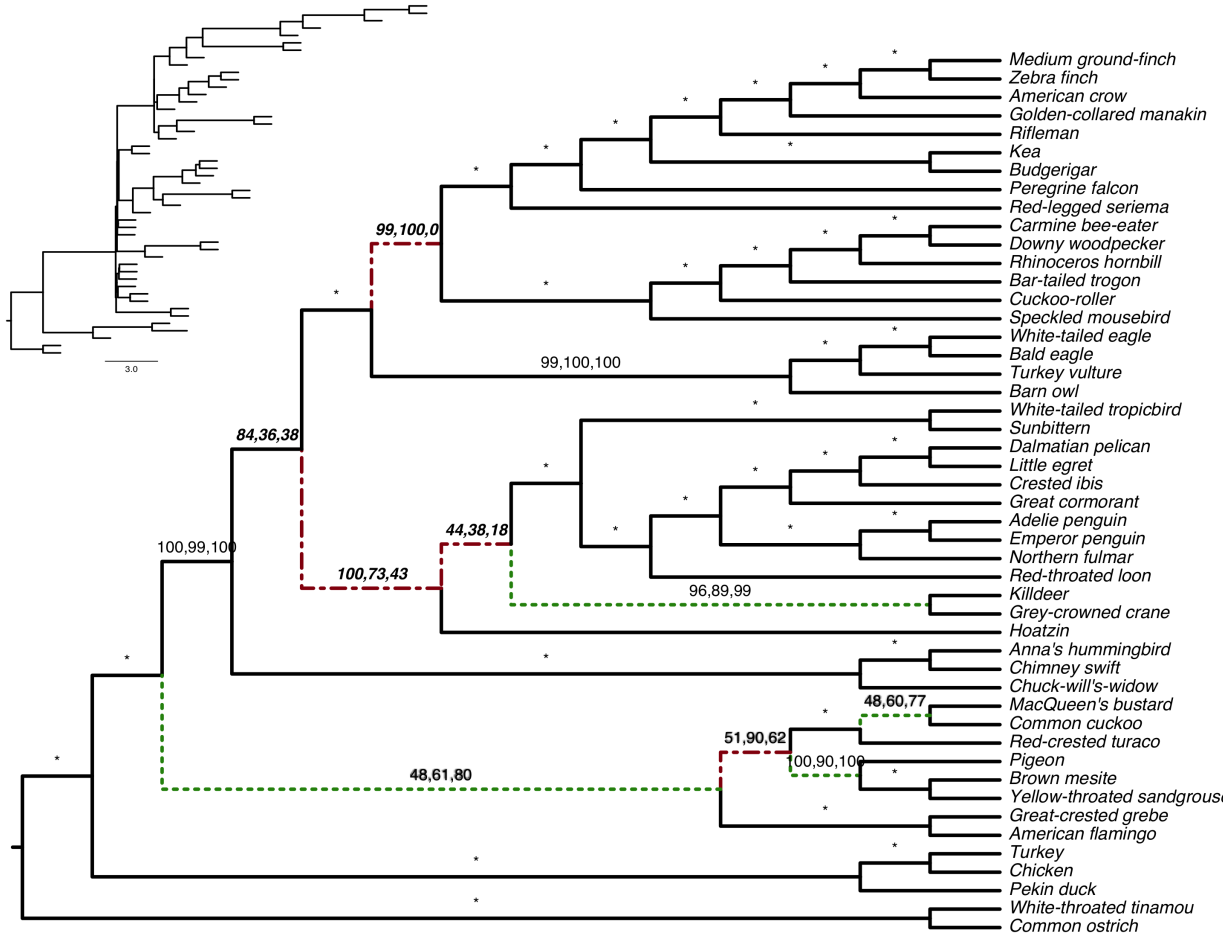


Figure S11: **Support on the avian dataset** Three forms of support values are shown for the avian dataset of Jarvis et al [4]. MLBS support (site-only), local posterior computed on fully ML resolved gene trees, and local posterior computed on ML gene trees with branches with less than 33% support collapsed. Branches marked with an asterisk (*) have 100% support with all three measures. Bold: local support on collapsed gene trees is at least 10% higher than MLBS support. Bold italic: local support on collapsed gene trees is at least 10% lower than MLBS support. Dotted/green lines (dashed/red lines): collapsing low support branches in gene trees increases (decreases) local posterior probability by at least 10%. Inset: branch lengths in coalescent units. The length of terminal branches are drawn arbitrarily.

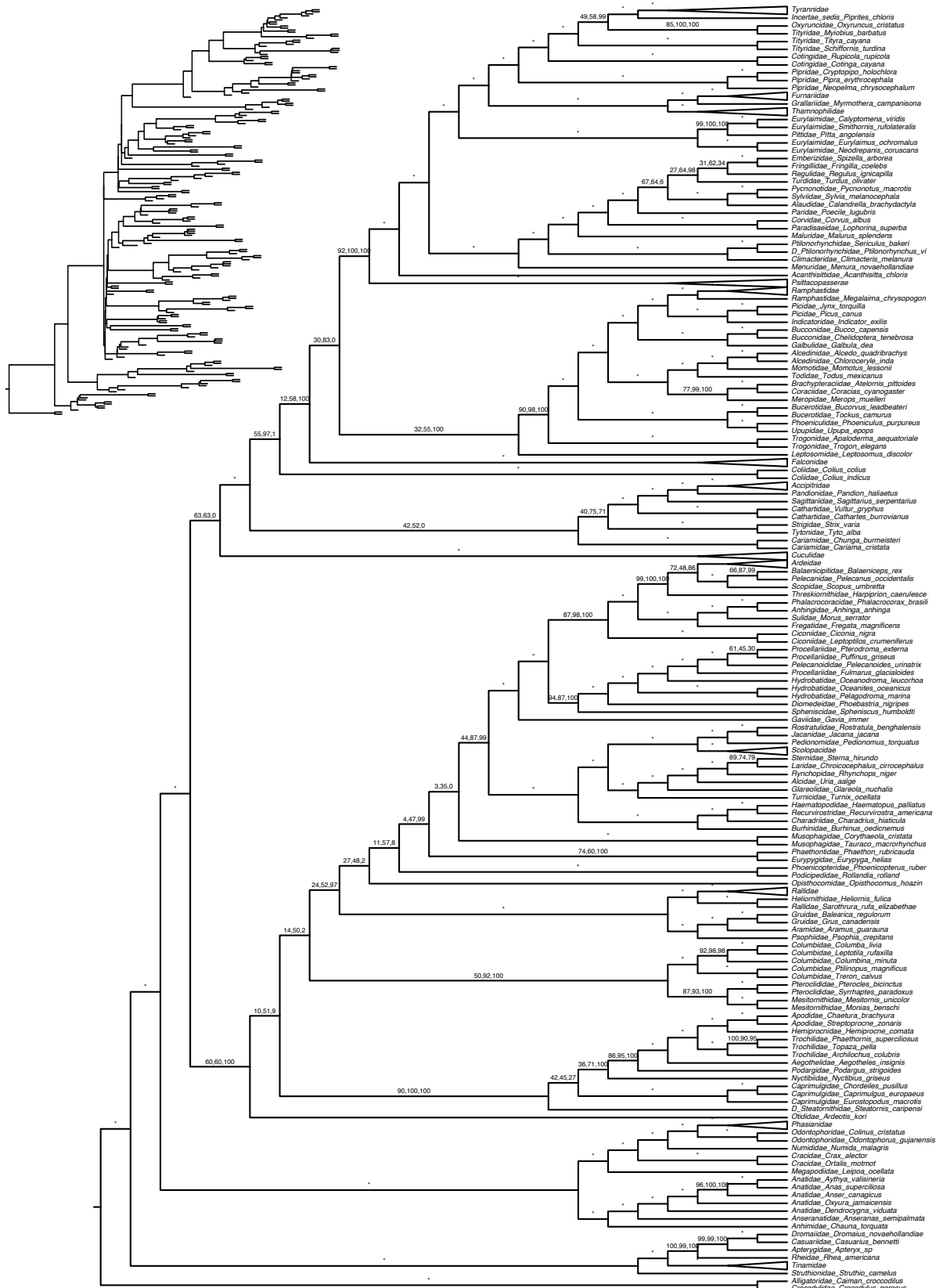


Figure S12: **Support on the avian dataset of Prum et al.** Three forms of support values are shown. Inset: branch lengths in coalescent units (terminal lengths are drawn arbitrarily). Collapsed clades had full support with all three methods for all branches.

```

function FREQ( $G, Q = (W, X)|(Y, Z)$ )
   $Q2 \leftarrow (W, Y)|(X, Z)$ 
   $Q3 \leftarrow (W, Z)|(X, Y)$ 
   $f1 \leftarrow F(G, Q)$ 
   $f2 \leftarrow F(G, Q)$ 
   $f3 \leftarrow F(G, Q)$ 
   $m \leftarrow (f1 + f2 + f3)/|G|$ 
  return  $(f1/m, f2/m, f3/m)$ 

function F( $G, Q = (W, X)|(Y, Z)$ )
   $r \leftarrow 0$ 
   $S \leftarrow$  empty stack
  for  $g \in G$  do
    for  $u \in postOrder(g)$  do
      if  $u$  is a leaf then
         $(w, x, y, z) \leftarrow (W[u], X[u], Y[u], Z[u])$ 
      else
         $(\mathbf{C}_{11}, \mathbf{C}_{12}, \mathbf{C}_{13}, \mathbf{C}_{14}) \leftarrow$  pull from  $S$ 
         $(\mathbf{C}_{21}, \mathbf{C}_{22}, \mathbf{C}_{23}, \mathbf{C}_{24}) \leftarrow$  pull from  $S$ 
         $(w, x, y, z) \leftarrow (\mathbf{C}_{11} + \mathbf{C}_{21}, \mathbf{C}_{12} + \mathbf{C}_{22}, \mathbf{C}_{13} + \mathbf{C}_{23}, \mathbf{C}_{14} + \mathbf{C}_{24})$ 
         $(\mathbf{C}_{31}, \mathbf{C}_{32}, \mathbf{C}_{33}, \mathbf{C}_{34}) \leftarrow (|W| - w, |X| - x, |Y| - y, |Z| - z)$ 
         $r \leftarrow r + I(\mathbf{C})$ 
      push  $(w, x, y, z)$  to  $S$ 
  return  $r/2$ 

function I( $\mathbf{C}$ )
  return

 $\mathbf{C}_{10} \times \mathbf{C}_{21} \times \mathbf{C}_{32} \times \mathbf{C}_{33} + \mathbf{C}_{11} \times \mathbf{C}_{20} \times \mathbf{C}_{32} \times \mathbf{C}_{33} + \mathbf{C}_{12} \times \mathbf{C}_{23} \times \mathbf{C}_{30} \times \mathbf{C}_{31} +$ 
 $\mathbf{C}_{13} \times \mathbf{C}_{22} \times \mathbf{C}_{30} \times \mathbf{C}_{31} + \mathbf{C}_{30} \times \mathbf{C}_{21} \times \mathbf{C}_{12} \times \mathbf{C}_{13} + \mathbf{C}_{31} \times \mathbf{C}_{20} \times \mathbf{C}_{12} \times \mathbf{C}_{13} +$ 
 $\mathbf{C}_{32} \times \mathbf{C}_{23} \times \mathbf{C}_{10} \times \mathbf{C}_{11} + \mathbf{C}_{33} \times \mathbf{C}_{22} \times \mathbf{C}_{10} \times \mathbf{C}_{11} + \mathbf{C}_{10} \times \mathbf{C}_{31} \times \mathbf{C}_{22} \times \mathbf{C}_{23} +$ 
 $\mathbf{C}_{11} \times \mathbf{C}_{30} \times \mathbf{C}_{22} \times \mathbf{C}_{23} + \mathbf{C}_{12} \times \mathbf{C}_{33} \times \mathbf{C}_{20} \times \mathbf{C}_{21} + \mathbf{C}_{13} \times \mathbf{C}_{32} \times \mathbf{C}_{20} \times \mathbf{C}_{21}$ 

```

Figure S13: **Frequency calculation algorithm.** Input is a set of gene trees G and a quadripartition $Q = (W, X)|(Y, Z)$ where each cluster (e.g., X) is a bitset indexed by the species (thus, $X[u]$ is 1 if leaf u is in X and otherwise is 0). Output is the quartet frequency for each of the three topologies around that branch.

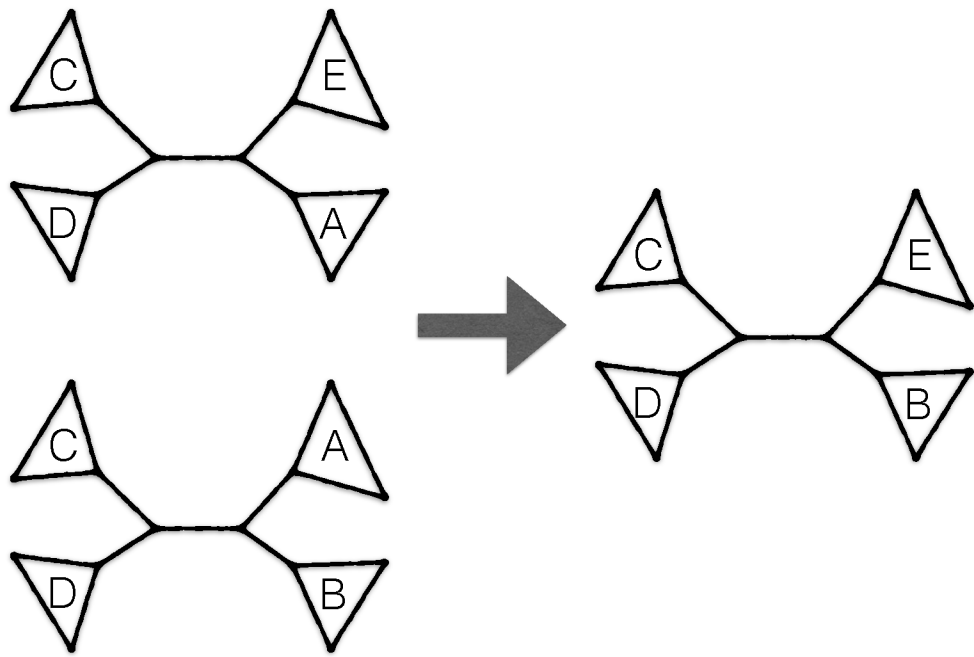


Figure S14: Topologies of different quartets around a branch might heavily depend on each other In this example, species A and B and E are closer to each other than each of them to C or D. Lets assume we observe topology of set of taxa A, B, C, D is $T_1 = A, B|C, D$ in a gene tree G , and the topology of set of taxa A, E, C, D is $T_2 = A, E|C, D$ in G . In this case the topology of set of taxa $T_3 = B, E|C, D$ is completely determined based on topologies T_1 , and T_2 . So it does not have extra information about the internal branch between them. To see this, imagine putting B on each of the five branches of $A, E|C, D$. Two branches (pending to C and B are not possible, because they contradict the other quartet topology. The other three placements all results in the $B, E|C, D$ topology.

2 Supplementary methods

3 Proofs

3.1 Proof of Lemma 1

Lemma 1 Let $(\theta_1, \theta_2, \theta_3)$ denote parameters of the true multinomial distribution generating F^* . Note $\sum_1^3 \theta_i = 1$ and the two lower θ_i s are identical, and recall f_1^* corresponds to the topology of Q .

$$Pr(\theta_1 > \frac{1}{3} | F^*) = \frac{\int_{\frac{1}{3}}^1 Pr(F^* | \theta_1 = t) Pr(\theta_1 = t) dt}{Pr(F^*)} \quad (S1)$$

with likelihood term:

$$Pr(F^* | \theta_1 = t) = \Gamma t^{f_1^*} (\frac{1-t}{2})^{k-f_1^*} = \Gamma g(f_1^*; t) \quad (S2)$$

where $\Gamma = \frac{\Gamma(k+1)}{\prod_1^3 \Gamma(f_j^* + 1)}$, and marginal probability:

$$\begin{aligned} Pr(F^*) &= \sum_{j=1}^3 \int_{\frac{1}{3}}^1 Pr(F^* | \theta_j = t) Pr(\theta_j = t) dt \\ &= \Gamma \sum_{j=1}^3 \int_{\frac{1}{3}}^1 g(f_j^*; t) Pr(\theta_j = t) dt. \end{aligned} \quad (S3)$$

Proof To prove Equation (S1), one could use Bayes' rule directly,

$$\begin{aligned} Pr(\theta_1 > \frac{1}{3} | F^*) &= \frac{Pr(\theta_1 > \frac{1}{3}, F^*)}{Pr(F^*)} = \frac{\int_{\frac{1}{3}}^1 Pr(F^*, \theta_1 = t) dt}{Pr(F^*)} \\ &= \frac{\int_{\frac{1}{3}}^1 Pr(F^* | \theta_1 = t) Pr(\theta_1 = t) dt}{Pr(F^*)} \end{aligned}$$

Equation (S2) comes from F^* being a multinomial distributed random variable given $\theta_1 = t$ is fixed and $\theta_1 > \frac{1}{3}$ (so $\theta_2 = \theta_3 = \frac{1-t}{2}$) directly. To prove Equation (S3),

$$\begin{aligned} Pr(F^*) &= Pr(F^* | \theta_1 > \frac{1}{3}) + Pr(F^* | \theta_1 \leq \frac{1}{3}) = Pr(F^* | \theta_1 > \frac{1}{3}) + Pr(F^* | \theta_2 > \frac{1}{3} \vee \theta_3 > \frac{1}{3}) \\ &= Pr(F^* | \theta_1 > \frac{1}{3}) + Pr(F^* | \theta_2 > \frac{1}{3}) + Pr(F^* | \theta_3 > \frac{1}{3}) \end{aligned}$$

3.2 Proof of Theorem 1

Theorem Given 1) a set of k gene trees generated by the MSC on a model species tree generated by the Yule process with rate λ and 2) an internal branch represented by a quadripartition Q where the four clusters around Q are each present in the species tree, let $F^* = (f_1^*, f_2^*, f_3^*)$ be the average quartet frequencies around Q (where f_1^* corresponds to the topology of Q); the local posterior probability that the species tree has the topology given by Q is:

$$Pr(Q | F^*) = \frac{h(f_1^*)}{h(f_1^*) + 2^{f_2^* - f_1^*} h(f_2^*) + 2^{f_3^* - f_1^*} h(f_3^*)} \quad (S4)$$

where

$$h(x) = \mathbf{B}(x+1, k-x+2\lambda)(1 - I_{\frac{1}{3}}(x+1, k-x+2\lambda)).$$

Here, $\mathbf{B}(\alpha, \beta)$ is the beta function, and I_x is the regularized incomplete beta function.

Proof F^* follows a multinomial distribution with parameters $(\theta_1, \theta_2, \theta_3)$. Lack of anomaly zones for unrooted quartets, shown by [5] means that Q is in the species tree iff $\theta_1 > \frac{1}{3}$. Thus, by Lemma 1 we can use (S1), (S2), and (S3) to compute the local posterior probability of Q . By the assumption that (coalescent unit) branch lengths in the species tree are generated by the Yule process, calculation of (S10) follows from manipulating (S1), (S2), and (S3), as detailed in the following Using Lemma 1,

$$Pr(\theta_1 > \frac{1}{3} | F^*) = \frac{\int_{\frac{1}{3}}^1 Pr(F^* | \theta_1 = t) Pr(\theta_1 = t) dt}{Pr(F^*)} \quad (\text{S5})$$

with likelihood term:

$$Pr(F^* | \theta_1 = t) = \Gamma t^{f_1^*} (\frac{1-t}{2})^{k-f_1^*} = \Gamma g(f_1^*; k, t) \quad (\text{S6})$$

where $\Gamma = \frac{\Gamma(k+1)}{\prod_1^3 \Gamma(f_j^*+1)}$, and marginal probability:

$$\begin{aligned} Pr(F^*) &= \sum_{j=1}^3 \int_{\frac{1}{3}}^1 Pr(F^* | \theta_j = t) Pr(\theta_j = t) dt \\ &= \Gamma \sum_{j=1}^3 \int_{\frac{1}{3}}^1 g(f_j^*; k, t) Pr(\theta_j = t) dt. \end{aligned} \quad (\text{S7})$$

In these equations $(\theta_1, \theta_2, \theta_3)$ denote parameters of the true multinomial distribution generating F^* , $\sum_1^3 \theta_i = 1$ and the two lower θ_i s are identical, and recall f_1^* corresponds to the topology of Q . Using (S7), and (S5),

$$Pr(Q | F^*) = \frac{\int_{\frac{1}{3}}^1 Pr(F^* | \theta_1 = t) Pr(\theta_1 = t) dt}{\Gamma \sum_{j=1}^3 \int_{\frac{1}{3}}^1 g(f_j^*; k, t) Pr(\theta_j = t) dt} \quad (\text{S8})$$

Based on Lemma 2, and Equation S2 $Pr(\theta_j = t) = \lambda(\frac{3}{2}(1-t))^{2\lambda-1}$, and $\Gamma t^{f_1^*} (\frac{1-t}{2})^{k-f_1^*}$. So Equation S8 simplifies to:

$$\begin{aligned} Pr(Q | F^*) &= \frac{\int_{\frac{1}{3}}^1 \Gamma t^{f_1^*} (\frac{1-t}{2})^{k-f_1^*} \lambda(\frac{3}{2}(1-t))^{2\lambda-1} dt}{\Gamma \sum_{j=1}^3 \int_{\frac{1}{3}}^1 \Gamma t^{f_j^*} (\frac{1-t}{2})^{k-f_j^*} \lambda(\frac{3}{2}(1-t))^{2\lambda-1} dt} \\ &= \frac{2^{f_1^*-k} \Gamma \int_{\frac{1}{3}}^1 t^{f_1^*} (1-t)^{k-f_1^*+2\lambda-1} dt}{\Gamma \sum_{j=1}^3 2^{k-f_j^*} \int_{\frac{1}{3}}^1 t^{f_j^*} (1-t)^{k-f_j^*+2\lambda-1} dt} \\ &= \frac{2^{f_1^*-k} \Gamma (\int_0^1 t^{f_1^*} (1-t)^{k-f_1^*+2\lambda-1} dt - \int_{\frac{1}{3}}^1 t^{f_1^*} (1-t)^{k-f_1^*+2\lambda-1} dt)}{\Gamma \sum_{j=1}^3 2^{f_j^*-k} (\int_0^1 t^{f_j^*} (1-t)^{k-f_j^*+2\lambda-1} dt - \int_{\frac{1}{3}}^1 t^{f_j^*} (1-t)^{k-f_j^*+2\lambda-1} dt)} \end{aligned} \quad (\text{S9})$$

With $\mathbf{B}(\alpha, \beta)$ as beta function, and I_x as the regularized incomplete beta function,

$$\mathbf{B}(x+1, k-x+2\lambda) = \int_0^1 t^{f_j^*} (1-t)^{k-f_j^*+2\lambda-1} dt$$

and,

$$\mathbf{B}(x+1, k-x+2\lambda) I_{\frac{1}{3}}(x+1, k-x+2\lambda) = \int_{\frac{1}{3}}^1 t^{f_j^*} (1-t)^{k-f_j^*+2\lambda-1} dt$$

then,

$$Pr(Q|F^*) = \frac{h(f_1^*)}{h(f_1^*) + 2^{f_2^* - f_1^*}h(f_2^*) + 2^{f_3^* - f_1^*}h(f_3^*)} \quad (S10)$$

where

$$h(x) = \mathbf{B}(x+1, k-x+2\lambda)(1 - I_{\frac{1}{3}}(x+1, k-x+2\lambda)).$$

3.3 Proof of Theorem 2

Theorem Under conditions of Theorem 1, and assuming the branch represented by Q is in the species tree, the ML estimate for its length is $-\ln \frac{3}{2}(1 - \frac{f_1^*}{k})$ and the MAP estimate is $-\ln \frac{3}{2}(1 - \frac{f_1^*}{k+2\lambda})$ when $3f_1^* \geq k$; otherwise, both ML and MAP are zero.

Proof With the assumption that the species tree is a Yule species tree, the branch length d is a random variable which is exponentially distributed, and $d \geq 0$. Assuming that Q be the true topology, the likelihood of d could be written as:

$$f_d(x; f_1^*, k) \propto (1 - \frac{2}{3}e^{-x})^{f_1^*} (\frac{1}{3}e^{-x})^{k-f_1^*} \quad (S11)$$

computing the log likelihood and removing the constants yields to:

$$L(x) = f_1^* \ln(1 - \frac{2}{3}e^{-x}) - (k - f_1^*)x \quad (S12)$$

The derivative of log-likelihood could be computed as:

$$\frac{dL^{ML}(x)}{dx} = \frac{f_1^* \frac{2}{3}e^{-x}}{1 - \frac{2}{3}e^{-x}} - (k - f_1^*) = 0 \quad (S13)$$

solving this gives the ML solution as $d_{ML}^* = -\ln(\frac{3}{2}(1 - \frac{f_1^*}{k}))$ if $d_{ML}^* \geq 0$, otherwise it is $d_{ML}^* = 0$. Note that $d_{ML}^* \geq 0$ if $\frac{3}{2}(1 - \frac{f_1^*}{k}) \leq 1$ or $\frac{f_1^*}{k} \geq \frac{1}{3}$, which means Q should be the dominant quartet topology in gene trees otherwise it is a very short branch and the ML estimate of its length is at boundary point 0.

The waiting time between the two consecutive speciation events is the length of the interior edge between them. Assuming that our species tree is a Yule tree, each species has a speciation rate λ , and this waiting time is exponentially distributed with mean $\frac{1}{2\lambda}$ [6] (proof of theorem 3.3). So for the MAP solution, we assume d is exponentially distributed with rate 2λ . In this case the posteriori could be written as:

$$f_d(x; f_1^*, k) \propto (1 - \frac{2}{3}e^{-x})^{f_1^*} (\frac{1}{3}e^{-x})^{k-f_1^*} e^{-2\lambda x} \quad (S14)$$

using similiar equations for ML, MAP solution is the solution of following equation:

$$\frac{dL^{MAP}(x)}{dx} = \frac{f_1^* \frac{2}{3}e^{-x}}{1 - \frac{2}{3}e^{-x}} - (k - f_1^* + 2\lambda) = 0 \quad (S15)$$

solving this gives the MAP solution as $d_{MAP}^* = -\ln(\frac{3}{2}(1 - \frac{f_1^*}{k+2\lambda}))$ if $d_{MAP}^* \geq 0$ otherwise it is $d_{MAP}^* = 0$. $d_{MAP}^* \geq 0$ if $\frac{3}{2}(1 - \frac{f_1^*}{k+2\lambda}) \leq 1$ or $\frac{f_1^*}{k+2\lambda} \geq \frac{1}{3}$.

3.4 Proof of Lemma 2

Lemma *If the species tree is generated using the Yule process with rate λ , branch lengths are exponentially distributed, and for $t \geq \frac{1}{3}$:*

$$Pr(\theta_j = t) = \lambda \left(3 \frac{1-t}{2}\right)^{2\lambda-1} \quad (\text{S16})$$

Proof Under the Yule process with rate λ , the branch lengths x are exponentially distributed with rate 2λ , and the pdf of x is $f_d(x) = 2\lambda e^{-2\lambda x}$ [6]. Note that because of absence of extra reliable information about the species tree topology, we use an uninformative prior, which means all topologies are equally likely to be the dominant one ($Pr(\theta_1 > \frac{1}{3}) = Pr(\theta_2 > \frac{1}{3}) = Pr(\theta_3 > \frac{1}{3}) = \frac{1}{3}$). Knowing that $\theta_j = 1 - \frac{2}{3}e^{-x}$ is in $[\frac{1}{3}, 1)$ as x goes from 0 to ∞ ($j = 1, 2, 3$), and by using the transformation rule of random variables:

$$Pr(\theta_j = t) = \frac{1}{3} \frac{1}{\left|\frac{d\theta_j}{dx}\right|} f_d(x) \Big|_{x=-\ln((1-t)\frac{3}{2})} = \lambda e^{(-2\lambda+1)x} \Big|_{x=-\ln((1-t)\frac{3}{2})} = \lambda \left((1-t)\frac{3}{2}\right)^{2\lambda-1}. \quad (\text{S17})$$

4 Commands and version numbers

We used ASTRAL version 4.9.1 available at <https://github.com/smirarab/ASTRAL/tree/posteval> for scoring and computing the branch lengths of the trees. To have posterior probabilities of branches of main species tree and 2 other alternatives we used:

```
java -Xmx2000M -jar astral.4.9.1.jar -i [GENE TREES] -q [SPECIES TREE] -t 4
```

To compute the branch lengths of main species tree we used the MAP solution with the command:

```
java -Xmx2000M -jar astral.4.9.1.jar -i [GENE TREES] -q [SPECIES TREE] -t 2
```

Users can find the most updated codes available at <https://github.com/smirarab/ASTRAL/tree/blen>. To score and compute the branch lengths, and local posterior probabilities of inferred species tree one can use:

```
java -Xmx2000M -jar astral.4.9.5.jar -i [GENE TREES] -q [SPECIES TREE] -t 3
```

References

- [1] DF Robinson and LR Foulds. Comparison of phylogenetic trees. *Mathematical Biosciences*, 53(1-2):131–147, 1981.
- [2] Siavash Mirarab and Tandy Warnow. ASTRAL-II: coalescent-based species tree estimation with many hundreds of taxa and thousands of genes. *Bioinformatics*, 31(12):i44–i52, jun 2015.
- [3] Zhenxiang Xi, Liang Liu, Joshua S Rest, and Charles C. Davis. Coalescent versus Concatenation Methods and the Placement of Amborella as Sister to Water Lilies. *Systematic Biology*, 63(6):919–932, nov 2014.
- [4] Erich D Jarvis, Siavash Mirarab, Andre J Aberer, Bo Li, Peter Houde, Cai Li, Simon Y W Ho, Brant C. Faircloth, Benoit Nabholz, Jason T Howard, Alexander Suh, Claudia C Weber, Rute R da Fonseca, Jianwen Li, Fang Zhang, Hui Li, Long Zhou, Nitish Narula, Liang Liu, Ganeshkumar Ganapathy, Bastien Boussau, Md. Shamsuzzoha Bayzid, Volodymyr Zavidovych, Sankar Subramanian, Toni Gabaldón, Salvador Capella-Gutiérrez, Jaime Huerta-Cepas, Bhanu Rekepalli, Kasper Munch, Mikkel H. Schierup, Bent Lindow, Wesley C Warren, David Ray, Richard E Green, Michael W Bruford, Xiangjiang Zhan, Andrew Dixon, Shengbin Li, Ning Li, Yinhua Huang, Elizabeth P Derryberry, Mads Frost Bertelsen, Frederick H Sheldon, Robb T. Brumfield, Claudio V Mello, Peter V Lovell, Morgan Wirthlin, Maria Paula Cruz Schneider, Francisco Prosdocimi, José Alfredo Samaniego, Amhed Missael Vargas Velazquez, Alonzo Alfaro-Núñez, Paula F Campos, Bent Petersen, Thomas Sicheritz-Ponten, An Pas, Tom Bailey, Paul Scofield, Michael Bunce, David M Lambert, Qi Zhou, Polina Perelman, Amy C. Driskell, Beth Shapiro, Zijun Xiong, Yongli Zeng, Shiping Liu, Zhenyu Li, Binghang Liu, Kui Wu, Jin Xiao, Xiong Yinqi, Qiuemei Zheng, Yong Zhang, Huanming Yang, Jian Wang, Linnea Smeds, Frank E Rheindt, Michael J Braun, Jon Fjeldsa, Ludovic Orlando, F Keith Barker, Knud Andreas Jónsson, Warren Johnson, Klaus-Peter Koepfli, Stephen O’Brien, David Haussler, Oliver A Ryder, Carsten Rahbek, Eske Willerslev, Gary R Graves, Travis C. Glenn, John E McCormack, Dave W Burt, Hans Ellegren, Per Alström, Scott V Edwards, Alexandros Stamatakis, David P Mindell, Joel Cracraft, Edward L Braun, Tandy Warnow, Wang Jun, M Thomas P Gilbert, and Guojie Zhang. Whole-genome analyses resolve early branches in the tree of life of modern birds. *Science*, 346(6215):1320–1331, dec 2014.
- [5] E S Allman, James H. Degnan, and J A Rhodes. Identifying the rooted species tree from the distribution of unrooted gene trees under the coalescent. *J. Math. Biol.*, 62:833–862, 2011.
- [6] Tanja Stadler and Mike Steel. Distribution of branch lengths and phylogenetic diversity under homogeneous speciation models. *Journal of Theoretical Biology*, 297:33–40, 2012.